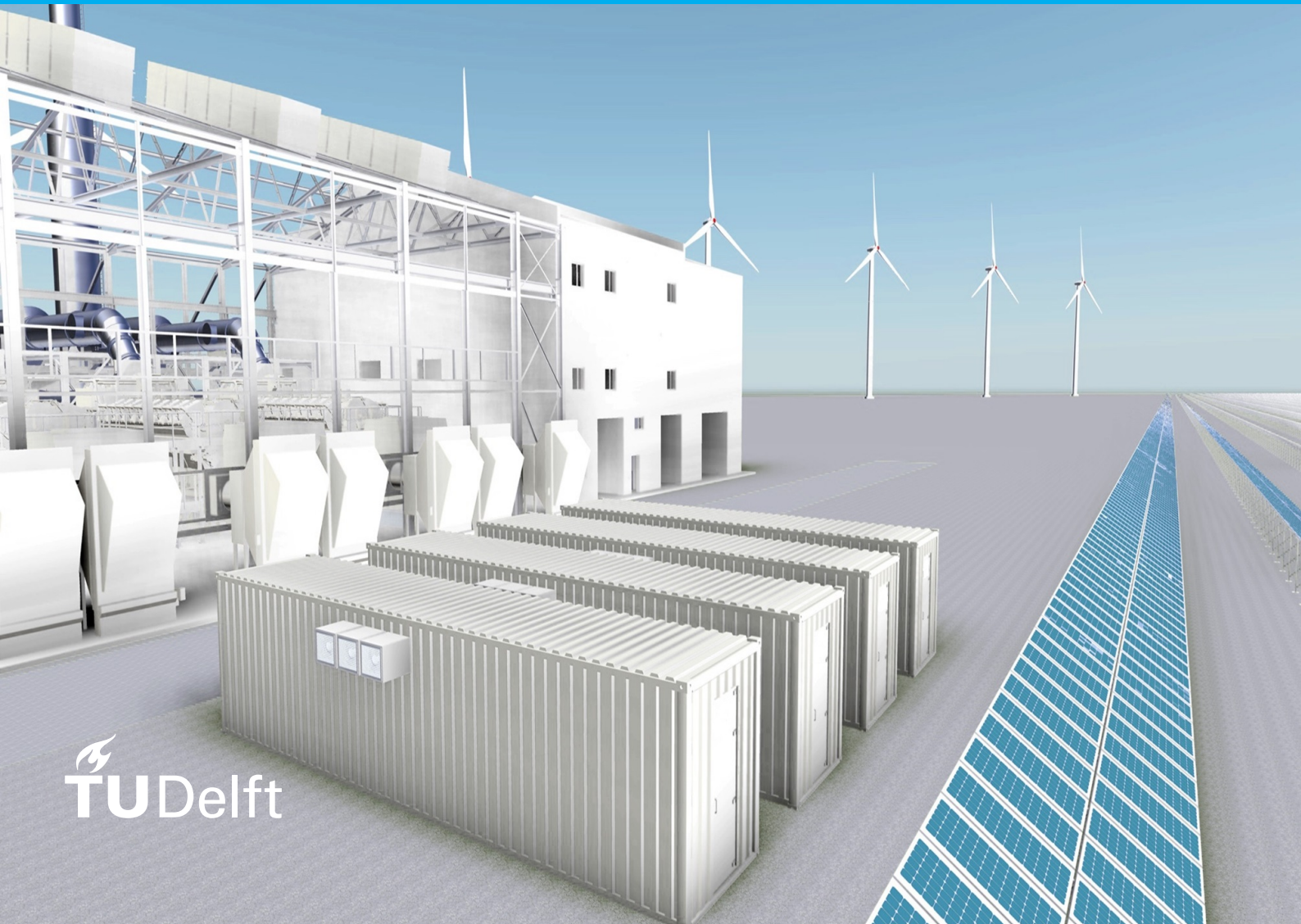


Investigating Hidden Flexibilities Provided by Power-to-X Consid- ering Grid Support Strategies

Master Thesis

B. Caner Yağcı

Intelligent Electrical Power Grids



Investigating Hidden Flexibilities Provided by Power-to-X Considering Grid Support Strategies

Master Thesis

by

B. Caner Yağcı

to obtain the degree of Master of Science
at the Delft University of Technology,
to be defended publicly on Tuesday August 26, 2020 at 15:00.

Student number: 4857089
Project duration: December 2, 2019 – August 26, 2020
Thesis committee:
Dr. Milos Cvetkovic, TU Delft, supervisor
Dr. ir. J. L. Rueda Torres, TU Delft
Dr. L. M. Ramirez Elizando TU Delft

This thesis is confidential and cannot be made public until August 26, 2020.

An electronic version of this thesis is available at <http://repository.tudelft.nl/>.



Preface

First of all, I would like to thank PhD. Digvijay Gusain and Dr. Milos Cvetkovic for not only teaching me the answers through this journey, but also giving me the perception of asking the right questions that lead simple ideas into unique values.

I would also like to thank my family Alican, Huriye, Uğur, Gökhan who have been supporting me from the beginning of this journey and more. You continue inspiring me to find my own path and soul, even from miles away. Your blessing is my treasure in life... My friends, Onurhan and Berke. You encourage me and give me confidence to be my best in any scene. You are two extraordinary men who, I know, will always be there when I need.

Finally, I would like to thank TU Delft staff and my colleagues in TU Delft for making this journey entertaining and illuminative for me.

*B. Caner Yağcı
Delft, August 2020*

Contents

List of Figures	vii
List of Tables	ix
1 Introduction	1
1.1 Background	1
1.2 Literature Review	2
1.2.1 Flexibility	3
1.2.2 Multi-Energy Systems	4
1.2.3 Energy Management of Multi-Energy Systems	7
1.3 Problem Definition	7
1.4 Previous Work	8
1.5 Research Questions & Objective	9
1.6 Research Approach	10
1.7 Outline	11
2 Methodology	13
2.1 Simulation Tools	13
2.1.1 OpenModelica	13
2.1.2 PandaPower	13
2.1.3 EnergySim	13
2.2 Considered Energy System	14
2.2.1 Energy Production	14
2.2.2 Energy Demand	16
2.3 Agent Based Hierarchical Control	17
2.4 Input Data	18
2.5 Analysis	20
2.5.1 Multi-Energy System Analysis	20
2.5.2 Power-to-X Model Analysis	20
2.5.3 Power System Analysis	20
3 Modelling	21
3.1 Industrial Loads	21
3.1.1 Power-to-Gas	21
3.1.2 Power-to-Heat	26
3.1.3 Electrical Base Load	30
3.2 Renewable Energy Sources	30
3.3 Electrical Network & Optimal Power Flow	30
3.3.1 Formulation of the Optimization Problem	31
3.4 Co-simulation Setup	32
4 Results & Discussions	33
4.1 Model Validation	33
4.1.1 PEM electrolyser model validation	33
4.1.2 Heat pump model validation	34
4.2 Analysis	35
4.2.1 Multi-Energy System Analysis	35
4.2.2 Power-to-X Model Comparison	36
4.2.3 Power System Analysis	39

5 Conclusion & Future Work	43
5.1 Conclusion	43
5.2 Recommendation for Future Work	43
A Historical Data Processing & Probabilistic Weather	45
B Wind Farm & PV Farm Data	47
C Ambient Temperature & Energy Demand Data	51
D R134a Pressure - Enthalpy Table	53
E Key Modelling Assumptions	55
E.1 Power-to-Gas	55
E.2 Power-to-Heat	55
E.3 Multi-Energy System	55
F Modelica Power-to-Gas Model Parameters	57
G Modelica Power-to-Heat Model Parameters	59
Bibliography	61

List of Figures

1.1 Energy-related carbon dioxide emissions with current policies compared to accelerated uptake of renewables (REmap), 2010–2050 [27]	1
1.2 Sources of power system flexibility [57]	3
1.3 An exemplary flexible load measure with the corresponding parameters [53]	4
1.4 Schematic illustration of main inputs, products, processes and technologies of different Power-to-X process chains and their classification [29]	5
1.5 Interconnections of power-to-heat options with electricity and district heating networks [10]	7
1.6 Shares of renewables in the energy mix of the power sector, the transport sector, and heat [48]	8
1.7 Communication between simulation tools	10
 2.1 Pandapower electrical network	14
2.2 Location of the 100 MW wind park in Maasvlakte	15
2.3 Location of the 100 MW solar park in Maasvlakte	15
2.4 Coupled multiphysic phenomena involved in an electrolysis stack [40]	16
2.5 Heating Cycle of Water	17
2.6 Flow chart of higher control level of MES	18
2.7 The relation between ambient temperature and hydrogen & heat demand [62]	19
 3.1 Power-to-gas model in OM	21
3.2 Electrolyser model "A" (upper) and model "B" (lower) model in OM	25
3.3 Adjustable power level controller in OM	26
3.4 Power-to-heat model in OM	27
3.5 Theoretical Single-Stage Vapor Compression Refrigeration Cycle ($C = \text{Constant}$) [16]	27
3.6 COP vs. T_{ambient} , $T_{\text{condenser}} = 70^\circ\text{C}$	29
3.7 COP vs. T_{ambient} , $T_{\text{condenser}} = 50^\circ\text{C}$	30
3.8 Co-simulation flow chart	31
3.9 Co-simulation synchronization	32
 4.1 PEM Electrolyser cell voltage vs. current density	34
4.2 Coefficient of performance (COP) vs. evaporating temperature for $T_{\text{cond}} = 50^\circ\text{C}$	34
4.3 Power capacity of renewable energy sources	35
4.4 Flexible demand of multi-energy system	35
4.5 Efficiency comparison of electrolyser models vs. time	36
4.6 Operational temperature comparison of electrolyser models vs. time	36
4.7 $P_{\text{Load},\text{PtG}}$ of electrolyser models vs. time	37
4.8 COP results of heat pump models vs. time	37
4.9 Ambient temperature vs. time	38
4.10 $P_{\text{Load},\text{PtH}}$ of heat pump models vs. time	38
4.11 P_{Load} results for Model "B" of PtG & PtH vs. time	39
4.12 Flexible active power demand of MES on 07.02.2019 for base case	39
4.13 Flexible active power demand of MES on 07.02.2019 for case 1	40
4.14 Hydrogen production of PtG models on 07.02.2019 for case 1	40
4.15 Heat production of PtH models on 07.02.2019 for case 1	41
4.16 Levelized cost of PtX for case 2	41
4.17 PtX active power consumption and Excess RE for case 2	42
 A.1 Historical data processing	45

List of Tables

1.1 Final energy consumption by sector, fuel (Mtoe) [3]	2
2.1 Ambient temperature - demand relation parameters	18
2.2 Cost considerations for PtG & PtH	19
2.3 Selected days for historical data	20
3.1 Modelling considerations of electrolyser	24
3.2 Hydrogen & Oxygen characteristics at 80 °C	25
3.3 COP results for various ambient and condenser temperatures	28
3.4 Modelling considerations of heat pump	28
3.5 5 th order polynomial fuction parameters for $T_{condenser} = 50, 70^\circ C$	29
3.6 Power-to-Heat storage parameters	30
3.7 Constraints	32

1

Introduction

The effects of climate change is clearly visible. Evolution to sustainable world is an urgent challenge that must be dealt by humankind for a better life. One of the best solutions of humankind to this problem is supplying energy demand by renewable energy sources (RES) such as wind, solar, etc. Those energy sources have low carbon emission for electrical power generation. However, stochastic nature of these RES puts reliability of existing electrical power system in great danger and introduces a new challenge for grid operators to match the energy demand and supply in the networks. As a result, flexibility of the electrical power system must be increased to allow larger percentage of RES in the electricity network and enhance reliability of the electrical power system.

1.1. Background

Zero-carbon emission is the ultimate goal of countries. For this reason, significant amount of renewable energy sources (RES) are integrated to the electricity network and more expected to be accommodated. Figure 1.1 shows energy-related carbon dioxide (CO_2) emissions with current policies compared to accelerated uptake of renewables until 2050. It is important to note, from this figure, that renewable energy and energy efficiency can provide up to 94% reduction in energy related CO_2 emissions. According to Paris Agreement [58], made by UN members, substantial greenhouse gas emission reductions are required across all sectors to mitigate the effects of climate change. The objective of the countries, by this agreement, is to keep the global temperature increase below 2°C and pursue efforts to keep it to 1.5°C for a progress towards climate- neutral economy with net-zero greenhouse gas emissions by 2050. In order to reach this objective, a worldwide effort to decarbonization the energy system, especially in industrial areas, is required.

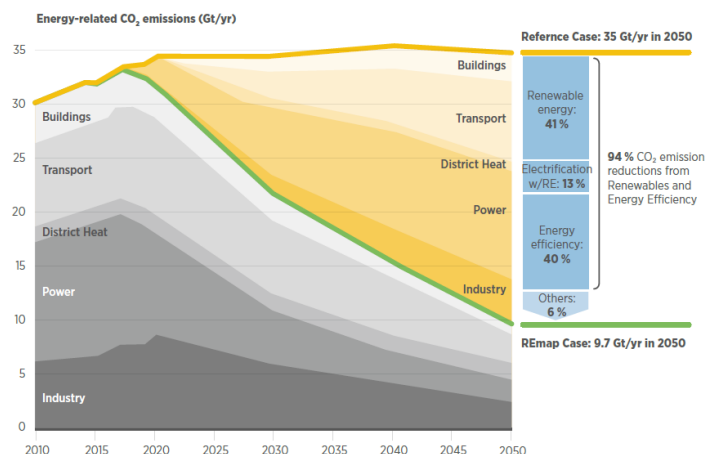


Figure 1.1: Energy-related carbon dioxide emissions with current policies compared to accelerated uptake of renewables (REmap), 2010–2050 [27]

Today, 35% of total energy demand is from industrial sectors globally [3]. Energy consumption per actor in industrial areas is much greater than that in residential or commercial areas. Electrification of even a few processes in industries can lead to significant amounts of carbon savings. Therefore, electrification of the industry is one the key ways to have energy transition pathway that may substantially contribute to a CO_2 neutral energy system. Conventional fossil fuel based generation units, have risen the carbon dioxide emissions dramatically. As a results, new electrically powered technologies and electrochemical processes being developed in order to increase the share of directly used clean renewable power in the power system. Table 1.1 reveals the increasing role of electricity compared to other fuels [3]. According to sustainable development scenario, electricity, direct use of renewables have the increasing interests in 2040. Increasing role of hydrogen in the future is also indicated in the table. It is mentioned that, this is due to increasing industrial gas demand and advantageous of hydrogen as an energy carrier (as explained in section 1.2.2). It is also noted from table 1.1 that, industry has the largest share among final energy consumption in 2040. Thus, electrification of the industry is the most promising way to increase energy system flexibility.

Table 1.1: Final energy consumption by sector, fuel (Mtoe) [3]

			Sustainable Development	
	2000	2018	2030	2040
By sector [Mtoe]				
Industry	1 881	2 898	2 949	2 904
Transport	1 958	2 863	2 956	2 615
Buildings	2 446	3 101	2 735	2 709
Other	758	1 092	1 264	1 272
By fuel [Mtoe]				
Electricity	1 092	1 915	2 349	2 902
District heat	248	296	264	224
Hydrogen	0	0	6	65
Direct use of renewables	271	482	887	1 142
Natural gas	1 127	1 615	1 816	1 719
Oil	3 124	4 043	3 695	2 838
Coal	542	984	746	533
Solid biomass	638	620	140	75

Reference [5] mentions that larger share of electricity from RES, especially from sun and wind, is increasing the flexibility demand of power system. Authors also point that, electricity demand as final energy will escalate due to the increasing penetration of Power-to-X technologies and this is the solution to increasing power system flexibility demand. Power-to-X (PtX) consists of electrically powered demand technologies such as electrolyzers, heat pumps (HP), electric vehicles, etc. and it allows coupling of electricity into various energy domains. It can be concluded from [5] that, these demand technologies, namely PtXs, also requires as much attention as RES have, and needs a detailed technical analysis before implementation. However, currently available models and methods in literature [28, 41], make significant simplifications on physical conditions of device, particularly in consideration of operational temperature and pressure conditions. Some other uses generic models that highly depend on manufacturer's data [56] and difficult to find for an industrial application. These simplifications made during modelling may lead to lose some of the essential dynamics for flexibility analysis such as correct efficiency characterization, ramp up/down characterization, etc. In reality, performance of a PtX highly depends on operational conditions. This means modelling of PtX technologies needs to be investigated according to the requirements of flexibility analysis. As a result, additional information obtained from detailed models during flexibility analysis is defined as the hidden flexibility of the P2X devices. It analyzes the effect of modelling simplifications on flexible load (PtX) performance.

1.2. Literature Review

This section is divided into three main parts. In the first part, flexibility in the literature is reviewed and flexibility in this project is defined. In the second part, multi-energy systems (MES) and two modelled power-

to-x (PtX) technologies are reviewed. Finally, in the third part, hierarchical control and optimal deployment of flexibility is reviewed with respect to multi-energy systems.

1.2.1. Flexibility

For reliable operation of electrical power system, energy balance between supply and demand must be maintained in any point of time. Electrical systems are able to deal with variability and uncertainty in both supply and demand of energy up to certain point, and this is called energy system flexibility [32]. However, integrating variable renewable energy sources such as wind or solar into electrical network increase the need for energy system flexibility.

Flexibility is quantified and classified in multiple ways depending on the nature of study being conducted. Reference [39] divides flexibility into four main parts: grid expansion, energy storage, flexibility on the supply side, and flexibility on the demand side; and defines demand-side flexibility as ability of a load to vary its scheduled profile. Supply side flexibility includes measures that can be taken to modify the output of power generation units for power balance. One of the ways for supply-side flexibility is curtailment of energy sources. Even though, curtailment of RES might be necessary during oversupply of RES, It also means losing electricity. Thus, it should be avoided by increasing the overall system flexibility from another aspect [32].

Reference [53] investigates industrial demand side flexibility of power consumption using generic data models. Data model provides standard description of a flexibility service that can be considered for different objects. This approach is useful for dealing with uncertainties in energy system. Reference [57] classifies flexibility sources as illustrated in figure 1.2. They focus on operational flexibility of power system by shifting the generation and demand profiles of resources. As can be understood from figure 1.2, flexibility of a system can be increased by controlling conventional power units, increasing storage capacity, demand response or curtailment of RES. Reference [47] proposes a taxonomy for modelling flexibility they simply define flexibility as the ability to deviate from the plan, and mention that flexibility of a given system is a unique, innate, state and time dependent quality. Examples show that different approaches can be taken while defining flexibility metrics, in order to analyse different aspects of electrical system.

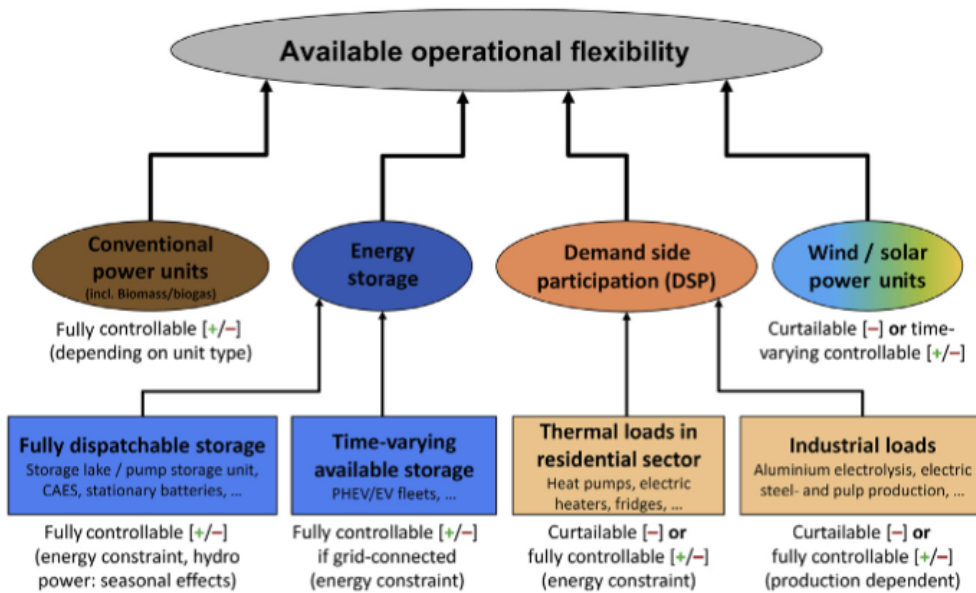


Figure 1.2: Sources of power system flexibility [57]

In this project, **flexibility is the ability of a component or a collection of components to respond to power fluctuations in power systems**. In this project, we look at Power-to-X devices, and the flexibility offered by them to support power system. From an operational perspective, PtX flexibility becomes relevant in situ-

tions where there is excess RE supply relative to demand in the power system and, therefore, electricity prices are low. During excess RE, power set-point of PtX can be elevated in order to provide flexible response and store this excess energy for low power generation times. Increasing the power consumption of PtX during excess RE provides power balance for electrical power system and reduces operational costs for PtX owners by providing opportunities to shift demand into low electricity price time.

Reference [53] mentions that, modelling of flexibility must be standardized in such a way that, models of components must describe flexibility potential as precisely as possible. Figure 1.3 shows the power consumption of exemplary flexible load with flexibility parameters. The key figures, that characterize flexibility, considered in this project are activation duration (t_{act}), holding duration ($t_{flex, on}$), deactivation period ($t_{restore}$) and power capacity [53]. Activation duration is the amount of time to reach flexibility set-point, and deactivation period is the amount of time to return to base set point and these parameters can be modelled or decided based on the inertia of the flexible system. Holding duration is the time duration in which the chosen power state will be hold. Additionally, storage level indication is inevitable for the flexibility characterization of storage models.

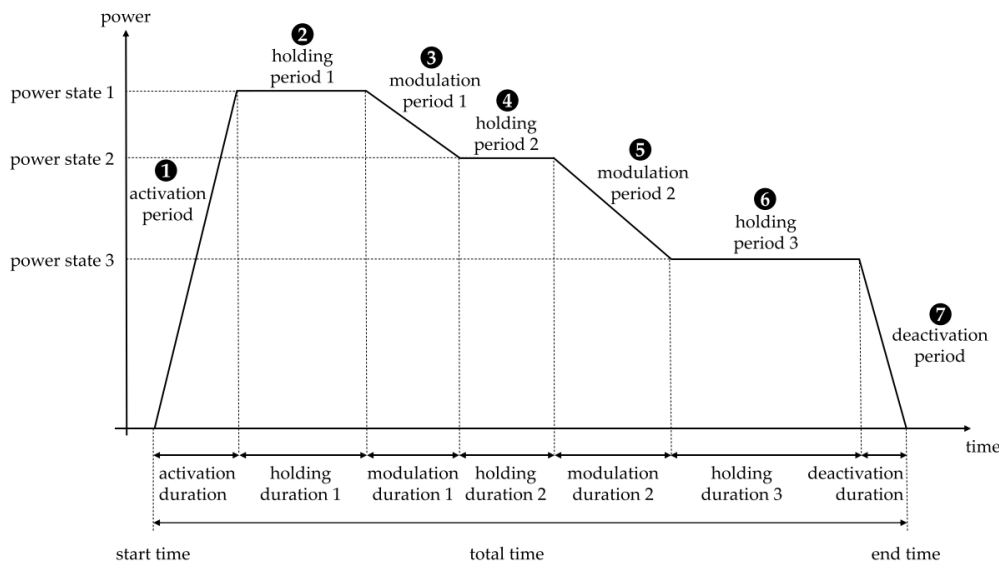


Figure 1.3: An exemplary flexible load measure with the corresponding parameters [53]

1.2.2. Multi-Energy Systems

In a multi-energy system, traditionally de-coupled energy vectors such as heat, electricity, gas, etc. optimally interact with each other at lower system levels, in order to enhance technical, economical and environmental performance of the system [33]. Reference [38] defines MES as the place where the production, conversion, storage and consumption of different energy carriers takes place. It is necessary to analyze inter-dependencies between these energy vectors in a MES, in order to optimally use them for sustainable, affordable and more flexible energy systems [34]. However, complex configurations of MES, with various PtX technologies available, makes this task challenging.

PtX technology is one of the key elements of a MES. It allows coupling of electrical power into various energy domains. Figure 1.4 illustrates some of the possible PtX chains. It reveals that various PtX technologies and their combinations exist in the industry. However, electrification of the entire energy system would be too complex, or at least much more expensive than combining renewable generation with low-carbon fuels [29]. Therefore, PtX should be selected according to needs of the energy system.

Hydrogen offers various ways for decarbonization, and power-to-hydrogen technology currently available to produce, store, transport or use hydrogen energy [2]. Reference [11] compares different combinations of MES and concludes that, a combination of PtG with electric heat pumps has the best cost performance

in a MES with renewables. Electrification of district heating systems considerably improves CO_2 emission reduction, because district heating/cooling demand, which mostly based on fossil fuels, sets for 45% of the final energy consumption globally, thus provides a great opportunity for greenhouse gas emission reduction [17, 30]. Table 1.1 shows that district heating demand shifts to direct use of renewables in sustainable development scenario. Additionally, high energy output of heat pumps with respect to approximately four times lower energy input makes PtH economical PtX option [29]. Subsections below explains why power-to-hydrogen and power-to-heat are considered for this research.

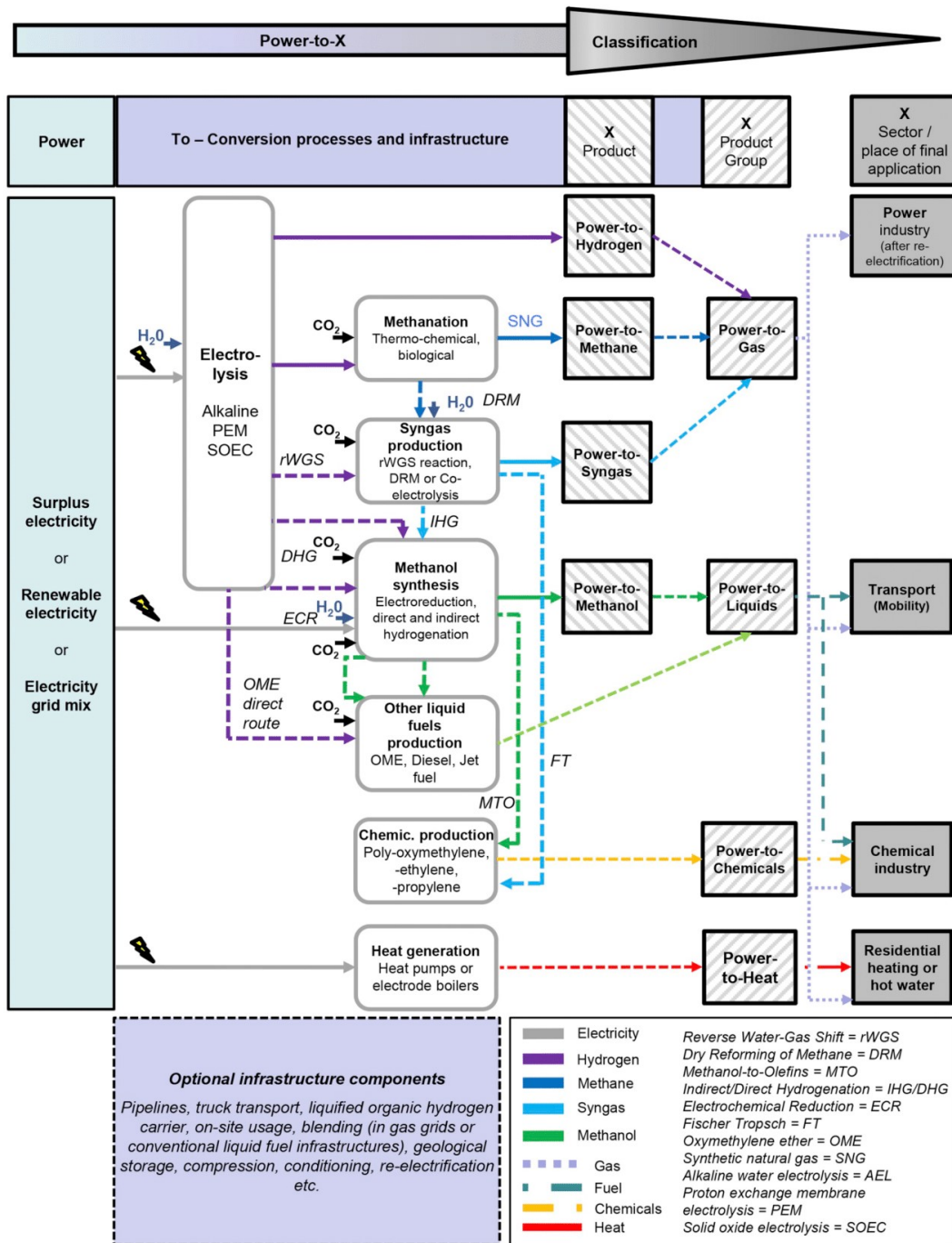


Figure 1.4: Schematic illustration of main inputs, products, processes and technologies of different Power-to-X process chains and their classification [29]

Power-to-Hydrogen (PtG)

Use of natural gas is decreasing as a result of clean energy transition. However, gases will remain crucial for a reliable, affordable and flexible energy system. Therefore, these gases must be produced with sustainable methods [31]. Hydrogen and green electrolysis may have a significant role in the production of zero-carbon gases [27]. Electrolysis is an electro-chemical process that uses direct electric current to split water molecules into hydrogen and oxygen. When RES is directly used for the the production of hydrogen this is called green hydrogen due to low carbon emissions. Currently, 4-5% of hydrogen is produced from electrolysis globally and the number of electrolysis plants is increasing. It is estimated that 270,000 tons of hydrogen will be produced in Northern Netherlands, between 2017 and 2030 to provide hydrocarbons to various sectors (industry, transportation, electricity, heating, etc.) [6]. Advantages of hydrogen as an energy carrier are listed below.

- Hydrogen is the lightest fuel in the nature, this means, it can be stored at high energy density with relatively smaller storage size than other gases. Therefore, hydrogen has a significant role on revealing the flexible capacity of MES, providing demand shifting opportunities with storage.
- Hydrogen can be produced from small-scale distributed electrolysis to large-scale, central electrolysis plants that could be integrated directly to renewable energy sources.
- No greenhouse gasses or other particulates are produced by the use/production of hydrogen with renewable energy sources.
- Hydrogen can be used for transportation sector by being stored in compressed gas tanks for applications similar to gasoline or propane.
- Hydrogen can be transported or stored in the existing gas distribution networks. Therefore, it does not require additional investments for capacity enhancements.
- Hydrogen can be formed into various hydrocarbons that used in variety of sectors (chemical, petro-chemical, etc.). Production of synthetic hydrocarbons from hydrogen would help greenhouse gas emission reduction by reducing the amount of fossil fuel used in that sector.

Power-to-Heat (PtH)

Compared to other PtX options power-to-heat is commonly practiced due to high coefficient of performance of heat pump and low heat storage cost [42]. Direct use of renewable energy sources in heating sector may reduce greenhouse gas emissions up to 40% globally [4], and provide additional flexibility to integrate more variable renewables into power system [10]. Figure 1.5 illustrates various PtH options with electricity and district heating networks. While centralized/industrial PtH units are connected to the heating network, decentralized PtH units do not support the existing heat network. Reference [36] proves that, large-scale heat pumps for district heating are especially promising if they operate efficiently in order to reduce the amount of excess electricity. Additionally, heat capacity of the heat pump system can be increased with an auxiliary boiler in order to improve performance [13]. Industrial heat compose 66% of industrial energy demand and approximately 20% of global energy demand. Most of the industrial CO₂ emissions is also caused from combustion of fossil fuels [25] in heat sector. Therefore, electrification of this sector would contribute to significant amount of carbon emission reduction. High efficiency can be reached for electrification of low or medium temperature industrial heat processes of heat pumps such as food, textile, tobacco plastics, etc [64]. Electrification of high temperature industrial processes such as steel,iron production can also be profitable depending on the application [25].

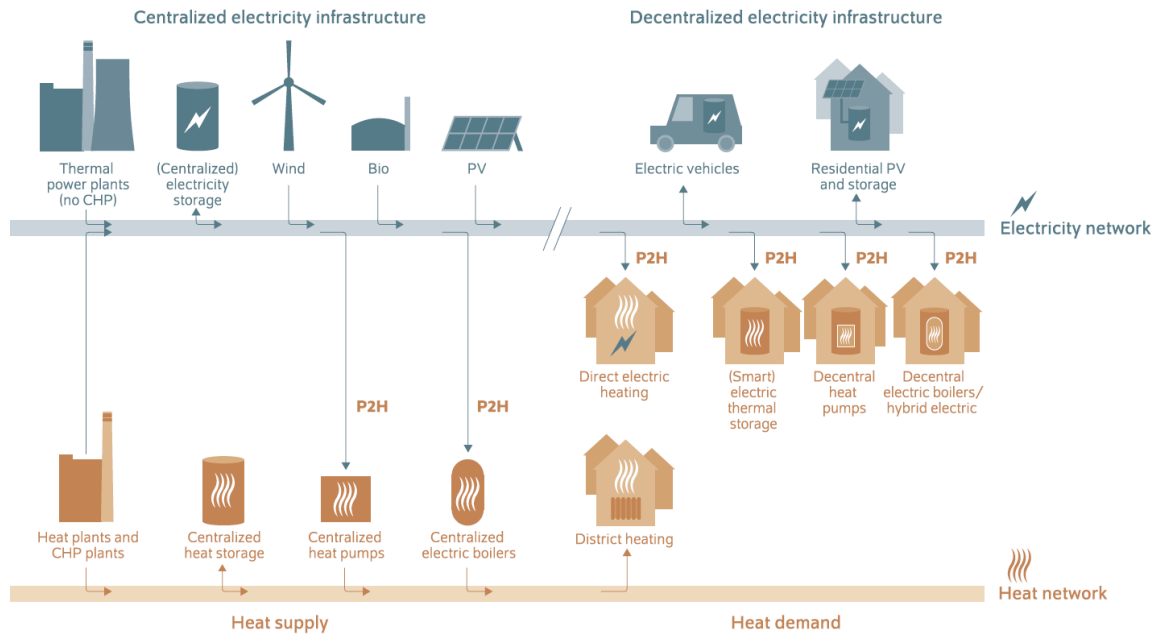


Figure 1.5: Interconnections of power-to-heat options with electricity and district heating networks [10]

1.2.3. Energy Management of Multi-Energy Systems

Energy management means optimizing the energy system for the optimal use of the available resources. Due to interconnections and dependencies between previously independent energy vectors, new control strategies are necessary for MES [51]. Even though technology required for hybridization of the energy system is already available at component level, system level influence of components and their resulting effects on power system still needs to be investigated [63]. In order to provide meaningful recommendations for MES, a holistic energy management approach is required that considers both physical and operational aspects. Reference [43] states that there is an increasing attention on demand-side management (DSM) to improve flexibility and categorize DSM into: energy efficiency of device, time of use rates, demand response (including market and physical demand response) and spinning reserve. They mention that a consideration for, at least, cost/price signals and physical demand response is necessary in order to make the optimal use of the available resources. Reference [34] indicates that flexible capacity can be provided by internally shifting the energy vectors inside MES, keeping the final energy demand of MES constant. They formulate an operational framework and optimisation problem to provide integrated ancillary services in MES.

By reason of distributed energy systems, control strategies at different levels of smart grid is essential to improve its reliability and sustainability [35]. Two or multi level configuration of energy management systems named as hierarchical control. With this approach, each component in the system considered as an agent that can communicate with the higher control level, namely community energy management system (CEMS), and CEMS can make decisions for the overall benefit of MES. A notable work on this topic is found in [14]. The authors in [14] mention that existing hierarchical management of MES models not considers energy cost of production (€/MWh). This results with unnecessary trading of electricity and increase in operational cost. Therefore, reference [14] proposes adjustable power level concept. According to adjustable power level information coming from agents, CEMS may directly control the generation amounts of PtXs in order to reduce the operational costs of MES by avoiding unnecessary trading with the utility grid.

1.3. Problem Definition

Figure 1.6 illustrates the expected share of RES in sectors. Although larger share of RES is expected in the future, highly volatile nature of these generation units reduces the reliability of power grid. In order to increase the percentage of RES in the electrical power system, the flexibility of the electrical network must be increased. Replacing production based on fossil fuels in chemical, petrochemical, food, steel and other industries leads to more sustainable and flexible multi-energy networks. However, in order to analyze MES a

technical analysis including their control, available flexibility, and optimal management & deployment must be carried out.

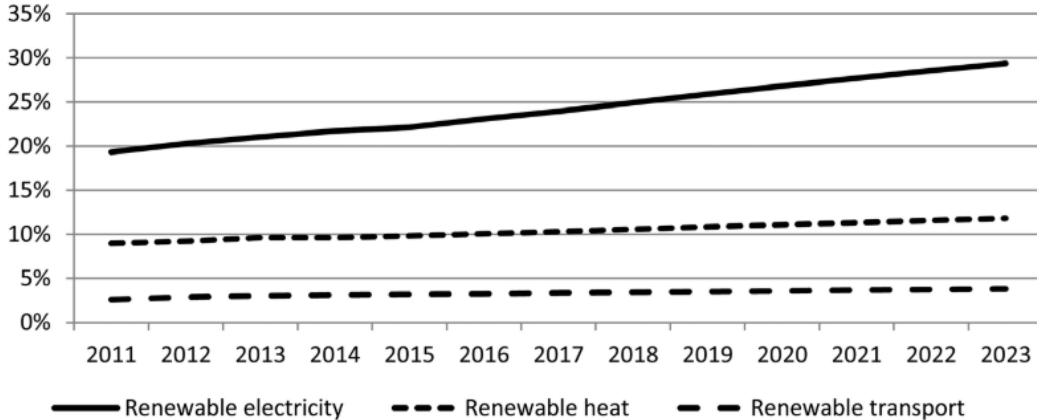


Figure 1.6: Shares of renewables in the energy mix of the power sector, the transport sector, and heat [48]

PtX models are simplified by single equations with constant or linear relation between the power input and energy output. However, operational performance of PtX such as electrolyser or electric heat pump strongly depends on operational temperature conditions. During flexibility analysis, this critical assumption leads to losing essential dynamics on simulation results. Correct efficiency characterization is crucial to understand the flexibility provided by Power-to-X, especially when a large number of these devices are present in the energy system. Inaccurate flexibility analysis of PtX may lead to increased transmission losses, higher operational costs or miscalculation of the MES capacity [53]. Due to simplifications made in model formulations, flexibilities provided by MES components to network can be concealed in the simulation results (hidden flexibility). Therefore, PtX modelling should be investigated to be optimally adapted to the requirements of flexibility analysis.

Another problem is, conventional energy management systems only consider generation side with limited amount of information. The planning and operation of multi-energy system needs to be coordinated to make optimal use of the available resources. Due to the inter-dependencies and connectivity between previously distinct energy vectors, a more holistic energy management and modelling approach must be provided including demand side management. However, this approach requires complex simulations to be set up. Even though reference [43] suggests that, a good combination of market demand response and physical demand response is necessary to run a network optimally, many of the existing simulation models for the energy management of MES do not have any information about the energy cost of other components in the network. This approach results in unnecessary trading of electricity with the utility grid and means an increase in operational cost for PtX owners [14]. Therefore, comprehensive energy management strategies that considers economical and physical aspects is needed to find the optimum operation point of MES.

1.4. Previous Work

Power-to-X technologies, especially electrolyser and electric heat pump, have the potential to be an integral part of an efficient, renewable and interconnected multi energy system. With respect to fuel cell systems, limited number of electrolyser model develop input-output models adapted to the requirements of control and flexibility analysis [40]. The existing generic electrolyser models use an efficiency curve to simulate the transformation of energy from power to gas [56]. While generic models are easy to simulate, they are highly dependent on manufacturer data or experimental measurements that are almost impossible to find for industrial systems. Thus, a lot of effort has to be performed in the modelling of detailed design of such systems. Several projects use partial differential equations for electrolyser modelling [28, 41]. These models are commonly used for mass transport behavior characterization. Some PEM electrolyser models available in the literature use ordinary differential equation (ODE) for efficiency characterization [18, 61]. ODEs are most commonly

used for practical applications of electrolyzers. Reference [18] characterize PEM electrolyzer physics and develops a detailed model of an industrial electrolyzer considering pressure, temperature, and current effects. This paper is chosen as the basis for modelling of the PEM electrolyser model.

During modelling of electric heat pump in MES, constant relation between power input and heat output is considered, assuming small variations of coefficient of performance (COP) over time [8, 9, 15, 23]. This assumption is made in order to reduce simulation complexity. However, in practice, COP of an heat pump strongly depends difference between inlet and the outlet temperature. Therefore, flexibility analysis requires more detailed electric heat pump models that considers effects of operational conditions on PtX performance. Diverse empirical approximations of heat pump's physical laws of operation can be made [60]. References [7, 13, 44] develop heat pump models with Carnot-COP, dependent on source and sink temperature. These papers are chosen as the basis for modelling of electric heat pump. The dependency of COP on both inlet and outlet temperature is taken into account by a polynomial fit in these two variables during modelling of heat pump. Additionally, several articles suggests using auxiliary electric boilers at the output of the heat pump system in order to increase the efficiency [11, 13]. The effect of auxiliary electric boiler on PtH performance is also considered during analysis.

Most of the research available on hierarchical energy management of MES do not have any information about the production cost of agents in the system. Most commonly, only excess and shortage amounts of PtX is considered, but cost signals of components in a MES are ignored during energy management analysis. Besides grid parameters and physical constraints, cost signals should also be considered in order to find the optimal operation point of MES. References [43] analyzes various types of energy management and demand-side management of intelligent energy systems. They mention that demand response (DR) of flexible load can be divided as Market DR and Physical DR, and consideration of both is required for the optimal operation of intelligent energy system. Reference [14] propose hierarchical energy management strategy based on multi energy system agents. They introduce adjustable power level concept in order to reduce operational cost.

1.5. Research Questions & Objective

The objective of this project is to investigate the impact of model fidelity of P2X devices in flexibility analysis. Additionally, impact of comprehensive energy management system to optimally control flexibility dispatch is investigated.

Research questions are divided into three main parts. First part considers PtX selection and flexible MES Design. Second part is about modelling of P2X to investigate impact of model fidelity. Finally the third part is about implementing hierarchical control to investigate the optimal deployment of flexibility.

The questions addressed in this research are:

- Which technologies have the highest potential to provide flexibility?
 - Which options are available in industrial area?
 - What are the options in order to increase flexibility of an industrial grid?
- To what extent does model fidelity impact flexibility analysis?
 - Which assumptions can be made and which physical effects should be considered?
- How to manage optimal deployment of flexibility considering individual resource constraints?
 - How to combine models representing different energy vectors efficiently?
 - How complex simulations can be created for energy management of MES?

The contribution of this thesis is two fold: firstly, investigating the effect of temperature simplifications of PtX models on flexibility analysis. Effects of auxiliary components on device performance is also

considered. Another contribution is the hierarchical agent based energy management approach considering leveledized cost signals with co-simulation.

1.6. Research Approach

First, literature review is conducted to analyze various PtX technologies. Their pros and cons are compared. Through extensive discussion, two of the most relevant technologies are selected. Next, specific characteristics of PtX technologies are studied and modelled using OpenModelica. Later, energy management system (EMS) is designed for optimal deployment of flexibility. Agent based hierarchical energy management system is considered. The aim of agent based hierarchical control is, besides grid parameters, considering physical constraints of agents and cost signals in order to find the optimal operation point of MES. After PtX models are created in OpenModelica (OM) and electrical network model with optimal power flow problem is created in Pandapower(PP), co-simulation is used to combine these models. Energysim is used for co-simulation. It allows to combine these two simulation software and implement complex control and flexibility analysis with multiple MES agents and a higher control level.

Modelling objective is to achieve an effective energy efficiency characterization during system's operation. PEM electrolyser model is created to study the performance behaviour of electrolyser under different operating conditions. An electrochemical steady-state model is created to calculate the stack/cell voltage and the stack/cell temperature evolution from instantaneous operating conditions such as the applied current, pressure and temperature. Temperature dynamics is added for detailed model version in order to compare the efficiency and performance behaviour of electrolyser model under different modelling assumptions. Pressure - Enthalpy table of ideal heat pump cycle working fluid (r134a) is used to characterize fifth order polynomial function of heat pump COP dependent on inlet and outlet temperatures. The aim of this modelling is to evaluate the performance of the heat pump with respect to different operational temperature assumptions and auxiliary electric boiler.

The aim of the agent based hierarchical energy management is to optimize the MES operation with respect to grid parameters, hydrogen/thermal comfort and energy cost. Optimization of the considered MES is carried out by Pandapower power flow solver. Optimal power flow solver calculates the exact operation point considering cost signals within the available power range defined by the physical situation of the Modelica agents. Hierarchical energy management is achieved with co-simulation by combining OM models with Pandapower solver in Energysim as illustrated in figure 1.7.

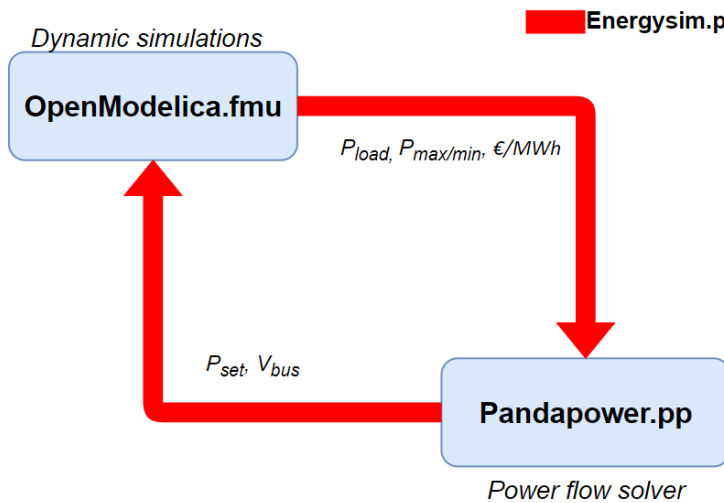


Figure 1.7: Communication between simulation tools

1.7. Outline

This report is divided into 5 chapters including introduction. Chapter 1, Introduction, explains research problem, research objectives and the literature review of the subject. Chapter 2, Methodology, describes key elements of the research approach, simulation tools and considered MES system. It also describes the input data preparation for simulations. Chapter 3, Modelling, describes the modelling of PtX and co-simulation setup. Chapter 4, Results & Discussion, presents the results obtained from models and simulation cases. Finally, chapter 5, Conclusion & Future Work, presents conclusions of the research and recommendations for future work.

2

Methodology

2.1. Simulation Tools

Three different software are used during project. Open Modelica (OM) is used for modelling of agents. PandaPower is used for power flow calculations of the electrical network, and these two software are combined in another, namely Energysim, for co-simulation and flexibility analysis.

2.1.1. OpenModelica

Modelica is an object-oriented, equation-based programming language which allows for dynamic simulations of multi-domain systems [37]. By reason of Modelica allows a physically based, dynamic simulation of the dynamic reactions; disturbances can be modelled and assessed. It also allows the combination of models coming from different technical domains in a unified way. A casual modelling of Modelica provides effortless modelling and fast simulation of complex dynamics. It also provides opportunity to export OM models as functional mock-up units for co-simulation. Thus, Modelica language is suitable to simulate coupled energy systems with different levels of detail. PtG and PtH with first order dynamics is modelled in OM as illustrated in figure 3.1, 3.4. These models can be further improved for faster or more detailed control and flexibility analysis of MES.

Various OpenModelica (OM) libraries, such as PowerGrids, PowerSystems, PVSystems, WindPowerPlants, AixLib, Buildings etc, have been considered in order to find the optimum balance between the simulation computation time, modelling simplicity and resolution of results. The controller models of PVSystems Library [46] has found useful for control analysis, but comes with increasing computation time. iTesla Power Systems Library (iPSL) [59] has decided to be the best option for the desired amount of simulation time and level of detail.

2.1.2. PandaPower

Pandapower is a python based open source tool for power system modeling, analysis and optimization with a high degree of automation. In this project, electrical network of MES is modelled using PandaPower [55] as illustrated in figure 2.1 and optimal power flow (OPF) solver of pandapower is used for the new setpoint calculation of MES components (PtX & RES). Costs, flexibilities and constraints are configured through the element-based pandapower data structure during optimal power flow. Pandapower allows to manage MES agents from higher control level with comprehensive energy management approach. During co-simulation, modelica agents (PtXs) sent maximum/minimum active power binding information and cost signals to pandapower for optimal power flow solver and the results of OPF sent as active power orders to PtX models via EnergySim for the initialization of the next macro timestep as illustrated in figure 3.8.

2.1.3. EnergySim

To evaluate the flexibility available from PtX and the impact that they can have on power system, complex simulations need to be set up [21]. Co-simulation is used for such complex system in order to implement hierarchical control, reduce computational burden and couple different energy domains. It provides more detail to manage & observe MES components during analysis and reduces simulation time by only using necessary

input and output. It allows complex control and flexibility analysis with multiple agents and a higher control level. There exist many co-simulation tools for MES that allow coupling of models from various energy domains, each with their pros and cons. Energysim (previously, FMUWorld) [21] is used for co-simulation. It is a python-based tool that was developed specifically to simplify energy system based co-simulations and focus on analysis by conceptualising the setup. It allows users to combine:

- Dynamic models packaged as Functional Mockup Units (FMUs)
- Pandapower Networks packaged as pickle files
- PyPSA models (BETA) packaged as Excel workbook
- csv data files

PtX models are tested on OpenModelica (OM) and exported as FMUs, using built-in FMU export function of OM. Pandapower network and optimal power flow solver is exported as pickle file. Co-simulation flowchart is illustrated in figure 3.8.

2.2. Considered Energy System

Figure 2.1 illustrates the considered MES. As can be seen, there is one industrial microgrid connected to external grid via 100 MVA transformer. Considered energy park is assumed to be 20 km away from the grid connection point. Power electronic converters are assumed to be ideal. In order to use excess renewable energy (RE) in district heating networks 50 MW district heating electric heat pump (with storage) and proton-exchange membrane (PEM) electrolyser (with storage) is connected to AC feeder. Having this MES design provides opportunity to compare both PtG and PtH options from various aspects (energy carrier, sector, performance, etc.).

Location and capacity of windfarm and PV farm are decided according to articles about Port of Rotterdam. The outer contour of Maasvlakte will be installed with 36 wind turbines, as illustrated in figure 2.2, and the installed capacity will be approximately 100 MW [52]. A floating solar park will be installed in Slufter, the installed capacity of PV farm will be approximately 100 MW_p [1]. Combination of these RES with the best available PtX technologies in the industrial area is assumed to be a "Hypothetical Energy Park in Maasvlakte 2".

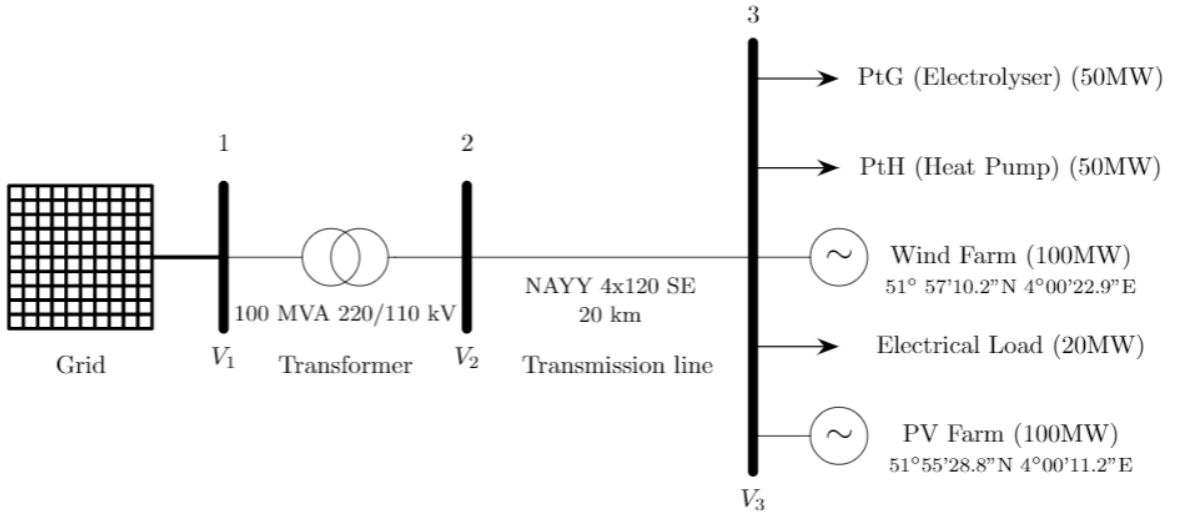


Figure 2.1: Pandapower electrical network

2.2.1. Energy Production

Figure 2.2 and 2.3 shows the location of the 100MW installed wind farm and the 100 MW installed PV farm respectively. The hourly power output of these RES are calculated from [48]. For generation profiles of 100

MW wind farm and PV farm at the indicated coordinates, see appendix B.

Windfarm details:

- Coordinates: 51°57'10.2"N 4°00'22.9"E
- Wind Turbine Generator: GE, 3.6MW, DFIG
- Number of wind turbines: 10 (3MW) (Harde Zeewering) + 26(3MW) (Zachte Zeewering)
- Capacity: 100-108 MW



Figure 2.2: Location of the 100 MW wind park in Maasvlakte

PV Farm details:

- Coordinates: 51°55'28.8"N 4°00'11.2"E
- PV Panel: 250 Wp
- Number of panels: 180.000<x<540.000
- Capacity: 45-135 MWp (apprx:100 MWp)



Figure 2.3: Location of the 100 MW solar park in Maasvlakte

2.2.2. Energy Demand

Considering most popular industrial PtX options in the literature and research gap in PtX modelling, power-to-gas with PEM electrolyser and power-to-heat with electric heat pump & auxiliary electric boiler are selected to be modelled in OpenModelica.

For 50 MW power-to-gas, proton-exchange membrane (PEM) electrolysis system with compressed hydrogen storage modelled in OM, as illustrated in figure 3.1. In order to model large scale electrolyser, it is assumed that electrolyser cells are assembled into stacks and connected in parallel for 50 MW capacity. Electrolyser model and empirical parameters in [61] is mainly used for modelling. Physical domains of electrolyser are divided into four domains: electrochemical, pressure, massflow and thermal. Each sub-model has input and output variables that connected to each other. This phenomena is illustrated in figure 2.4 and models are shown in figure 3.2.

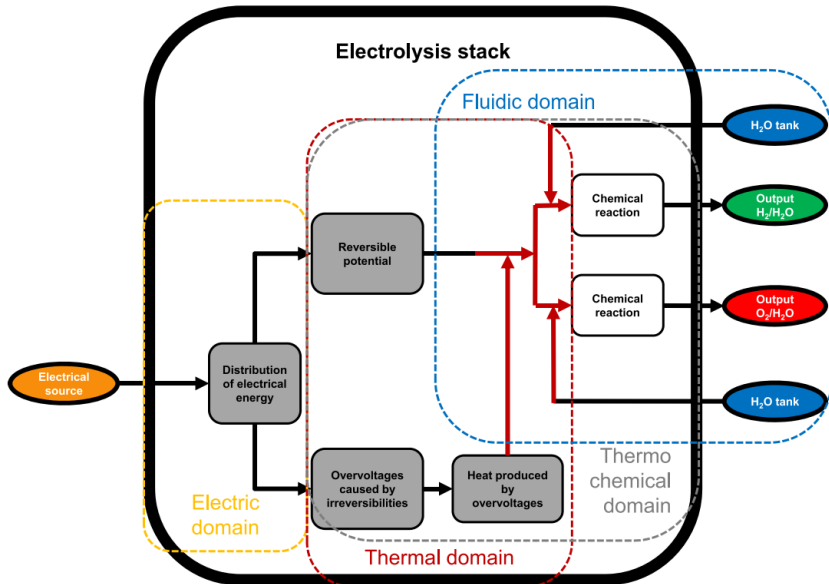


Figure 2.4: Coupled multiphysic phenomena involved in an electrolysis stack [40]

In reality, electrolyser cell is not able to provide favorable operation of electrolysis on its own. Therefore, electrolyser system must include auxiliary components for temperature regulation, input/output conditioning and power regulations. In order to investigate the effect of temperature evolution on electrolyser performance, auxiliary components are considered for the electrolyser thermal sub-model. Additionally, energy level of a gas tank is calculated from the available volume assuming the tank pressure & temperature remains constant without losses.

For 50MW power-to-heat, district heating electric heat pump with hot water storage and auxiliary electric boiler modelled in OM. The thermal efficiency of the heat pump is characterized as coefficient of performance (COP). COP is the ratio of heat produced over input power, which is the electric compression work of heat pump in this case. Thermal efficiency of a heat pump depends on the rankine cycle of refrigerant inside. Refrigerant R134a, that commonly used in district heating electric heat pumps [50], is assumed to be used in this heat pump. As a result, Pressure-enthalpy table of R134a (given in appendix D) is used for the calculation of COP at various inlet and outlet temperatures. Later, COP results are used in Matlab curve fitting in order to generate fifth order polynomial equation that calculates COP of heat pump rankine cycle (Carnot COP) depending on ambient and condenser temperature.

For district heating, hot water delivered at 70 °C and return temperature at T_{amb} are assumed. Electric heat pump is entitled as the main heat producer for all cases. For model C (explained in section 3.4), a 15MW auxiliary electric boiler is activated at full load when ambient temperature is lower than 15 °C in order to support heat pump during low ambient temperatures, by reducing the temperature difference between the inlet

and outlet of heat pump for efficient operation. In this case, when the boiler is activated, heat pump outlet temperature is switched from 70 °C to 50 °C for higher COP. Hot water cycle is illustrated in figure 2.5.

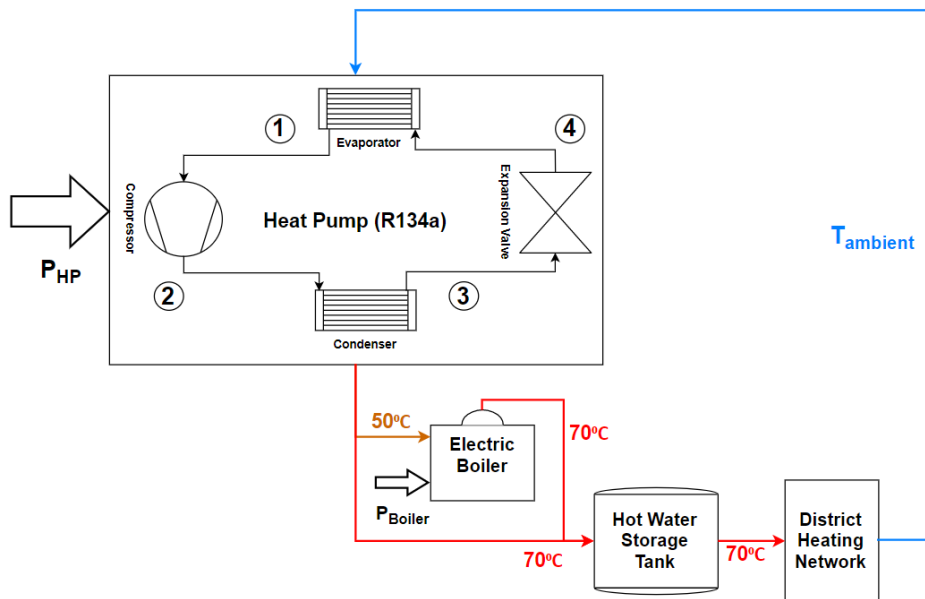


Figure 2.5: Heating Cycle of Water

5 kg per second constant massflow between the heat pump and the storage is assumed for district heating hot water and compressor power of heat pump is controlled with respect to district heating demand. To increase flexibility of MES, a hot water storage tank is connected in P2H to district heating network. It is assumed that the storage tank is able to hold 2400 m³ of 70 °C water without any losses [50].

2.3. Agent Based Hierarchical Control

Pandapower (PP) power flow slow solver is used for the energy management of MES at higher control level. Optimal power flow calculation finds the optimal values of active power set points of MES agents to achieve minimum operating cost, as illustrated in figure 2.6. At lower control level, local objective of MES agents, namely PtG and PtH models, is to supply demand at all times through P_{min} output of adjustable power level controller. At higher control level, global objective of the optimal power flow is to minimize operational costs considering leveled cost signals and binding information (flexibility constraints) (P_{min}, P_{max}) coming from OM agents. In order to do this, built-in optimal power flow solver of pandapower is enhanced by combining with OM models in Energysim. PP has to communicate with the OM agents and learn the operational active power constraints, that is the flexibility constraints, and leveled cost signals (as explained in section 2.4) in order to calculate the optimum operation point within this range.

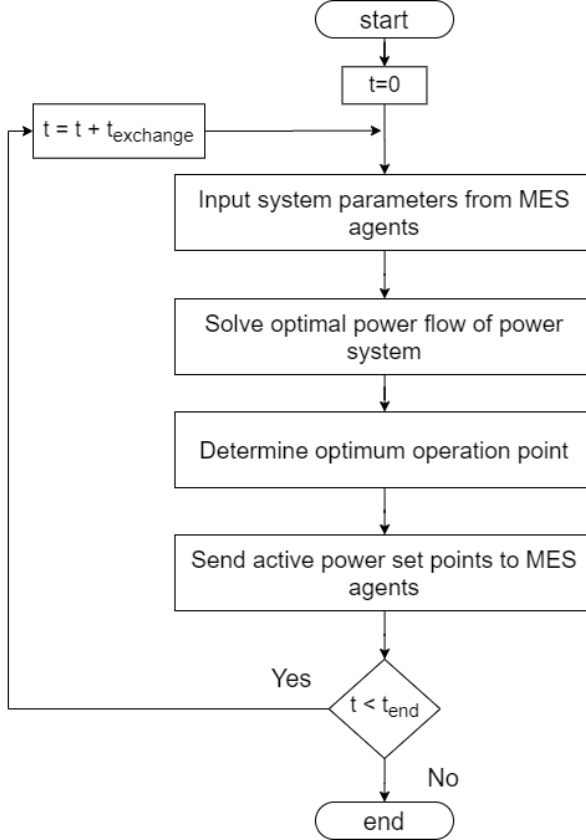


Figure 2.6: Flow chart of higher control level of MES

2.4. Input Data

Scheduled (Static) Energy Demand Profiles

In order to characterize storage flexibility, timeseries scheduled energy demand profiles are created. Those are the discharge rate of storage unit in each PtX model. As can be imagined, hourly timeseries heat or hydrogen demand data for industrial networks is exceptionally publicly available. Therefore, model of [19] is used to achieve this task based on the local temperature. Equation 2.1 uses ambient temperature data to determine the share of the dependency of a demand on temperature. In figure 2.7, Q_0 is the base demand which occurs at temperatures above the reference temperature T_R . Q_{max} is the maximum heat demand corresponding to the minimum temperature T_{min} . District heating networks is expected to be very sensitive to ambient temperature changes. On the other hand, industrial hydrogen demand is expected to be less dependent on the ambient temperature. Therefore the slope of the linear line in figure 2.7 is bigger for Power to Heat than Power to Gas. This means, industrial hydrogen demand has less variations with respect to varying ambient temperature than district heating demand. Values of the parameter are shown in table 2.1.

$$Q(t) = Q_0 + \frac{Q_{max} - Q_0}{T_R - T_{min}} \max(0, T_R - T(t)) \quad (2.1)$$

Table 2.1: Ambient temperature - demand relation parameters

	$T_{Reference}$ [°C]	T_{min} [°C]	Q_0 [m_3/s]	Q_{max} [m_3/s]
Industrial PtG	25	5	3.1372e-03	3.8502e-03
District Heating PtH	25	5	3	4

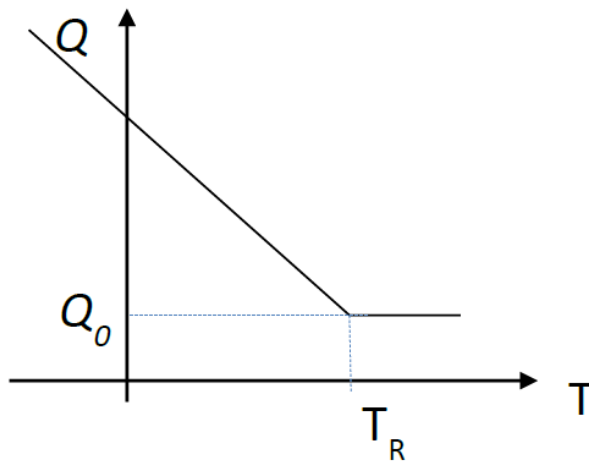


Figure 2.7: The relation between ambient temperature and hydrogen & heat demand [62]

Levelized Cost of Energy Production

Linear Euro per MWh cost signals that sent to pandapower are calculated as in equation 2.2, 2.3. Improvements on MES energy performance and reduction in carbon emissions was the primary considerations for levelized cost of energy equation. The values in table 2.2, that used for the equations, are from [11]. Carbon emission factors are decided considering green electrolysis pathways and electric heat pump district heating pathways [24, 26, 45]. What should be noted from these equations is, instead of energy produced over lifetime on denominator of levelized cost equation, instant efficiencies of models are used. This way cost of energy production of each PtX is compared for the optimal energy management of MES with respect to their efficiencies and carbon emissions. Both PtX use the same fuel which is renewable electricity and it is assumed to be the cheapest fuel during excess RE. Carbon price is also assumed to be same for both model; therefore its value is 1.

$$\text{Levelized cost of hydrogen} = \frac{\left(\frac{\text{CAP+O\&M}}{\text{LT}[a]}\right)_{\text{Electrolyser}} + \text{Carbon penalty}}{\text{efficiency}(t)} \quad (2.2)$$

$$\text{Levelized cost of heat} = \frac{\left(\frac{\text{CAP+O\&M}}{\text{LT}[a]}\right)_{\text{HP}} + \left(\frac{\text{CAP+O\&M}}{\text{LT}[a]}\right)_{\text{Boiler}} + \text{Carbon penalty}}{\text{COP}(t)} \quad (2.3)$$

$$\text{Carbon penalty [EUR/kW]} = \text{CO}_2 \text{ emission factor [g CO}_2 \text{ kW}^{-1}] \times \text{Carbon price [EUR g CO}_2^{-1}] \quad (2.4)$$

Table 2.2: Cost considerations for PtG & PtH

	Electrolyser	Electric Heat Pump	Electric Boiler
CAPEX [EUR/kW]	200	1000	70
O & M [EUR/kW]	8	35.5	1.4
Lifetime [a]	20	20	15
Carbon emission factor [gCO₂/kWh]	16.6	62.3	-
Carbon penalty [EUR/kW]	16.6	62.3	-

2.5. Analysis

This section explains the analysis considered in order to understand the MES phenomena and answer the research questions in section 1.5. The year of 2019 is divided into 8 sections of 45 days. As a result, 8 days from 2019 is selected for the analysis to represent the year of 2019. Later, one of the days is selected for power system analysis. Table 2.3 shows considered days for historical data and each day is indicated by vertical dashed line on figures of the results part. Hidden flexibility is quantified, by comparing the created models, from the final active power demand of MES on power system scale and from the amount of energy output of PtX on model scale.

Table 2.3: Selected days for historical data

Selected Days for Historical Data
07.02.2019
23.03.2019
07.05.2019
23.06.2019
07.08.2019
23.09.2019
07.11.2019
23.12.2019

2.5.1. Multi-Energy System Analysis

MES analysis is carried out in order to investigate the seasonal weather behaviour in the area and investigate the flexible capacity of industrial MES with selected flexible loads. According to the results of this part, one of the considered days is selected for 24 hours power system analysis, explained in section 2.5.3.

2.5.2. Power-to-X Model Analysis

In this part, temperature evolution and efficiency characters of considered models are compared in order to investigate the effect of modelling considerations on device performance. Later, effects of these models on power system are compared in power system analysis.

2.5.3. Power System Analysis

In this part, in order to investigate the influence of modelling considerations on power flow results, PtG and PtH models are combined with pandapower power flow solver using co-simulation. Flexibility is quantified by the final energy demand of MES. Final energy demand is the difference between the total energy demand and total RES generation of MES. This means, final energy demand of a desired self-sufficient MES would be zero or lower than zero (excess RE) at all times; however, if the RES capacity is lower than demand than final energy demand of MES would be positive, which means MES would require energy from outside.

- **Base case:** In this case, it is assumed that none of the PtX is available for flexibility service. Without any flexibility service, measuring the flexible demand of MES and proposing holding duration for flexibility service.
- **Case 1:** In this case, only one P2X (either PtG or PtH) is available for flexibility service. During flexibility service, active power set-point of PtX is switched to nominal power for a pre-defined holding duration decided in the base case. Comparing both PtX options with respect to reduction in flexible demand of MES after flexibility service. Comparing the energy output of created models for a given flexibility request.
- **Case 2:** This case is to investigate the optimal deployment of flexibility. Both P2X's are available for flexibility service. Considering leveled cost signals and adjustable power level constraints, measuring the amount of shared flexibility between P2G & P2H and quantifying the reduction in total operational cost.

3

Modelling

3.1. Industrial Loads

Industrial loads modelled in this project are power-to-gas (PtG), including PEM electrolyser and compressed hydrogen storage tank; and power-to-heat (PtH), including electric heat pump and hot water storage tank for district heating network. Additionally, both PtX have static generator model for electrical interface and adjustable power level controller explained in section 3.1.1.

3.1.1. Power-to-Gas

Figure 3.1 shows modelled power-to-gas system. The inputs of the model are scheduled industrial hydrogen demand that defines minimum active power and ambient temperature. In addition to these, active power set points to control electrolyser hydrogen output and/or voltage set point for reactive power control can be used. Details of each model are explained below.

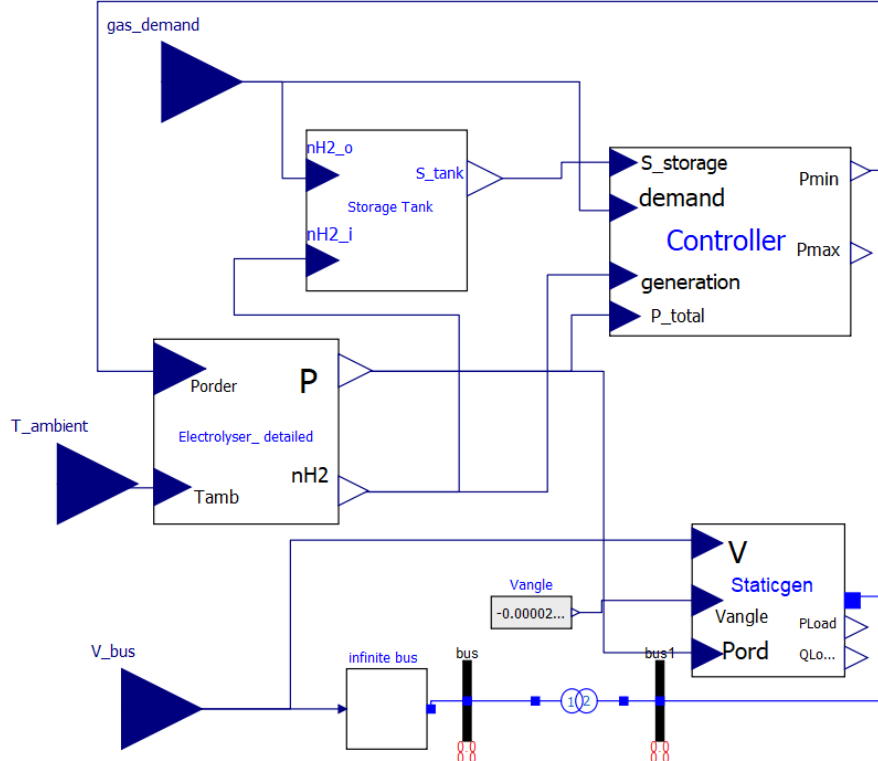


Figure 3.1: Power-to-gas model in OM

Electrolyser

PEM electrolyser cell voltage and power is characterized in electrochemical sub-model with equations 3.1-3.9.

Electrochemical:

$$V_{cell} = V_{ocv}(T, p) + V_{act}(T) + V_{ohm}(T) \quad [V] \quad (3.1)$$

Open-circuit voltage, V_{ocv} , is the voltage necessary to start the water electrolysis reaction under ideal conditions. It is calculated using Nernst equation 3.2. In this equation, T_{op} is the stack average temperature between the inlet and the outlet of the anode side, pp_{H2O} is the water partial pressure, and pp_{H2} and pp_{O2} are the hydrogen and oxygen partial pressures in the hydrogen and oxygen gas separators, respectively. R , F is ideal gas constant and faraday constant, respectively. Reversible cell voltage is calculated as in equation 3.3. V_{std} is 1.23 V for PEM water electrolysis, and standard temperature T_{std} is 298.15 °K. Coefficient of temperature difference is calculated in [18].

$$V_{ocv} = V_{rev} + \frac{R \cdot T_{op}}{2 \cdot F} \cdot \ln \left(\frac{pp_{H2} \cdot pp_{O2}^{0.5}}{pp_{H2O}} \right) \quad [V] \quad (3.2)$$

$$V_{rev}(T_{op}) = V_{std} - 0.0009(T_{op} - T_{std}) \quad [V] \quad (3.3)$$

Energy losses within the PEM stack can be modelled as overpotentials. Activation overpotential, V_{act} , is the energy necessary to start the electrochemical reaction. It is dominant at low current densities. Here, i_{dens} is the current density of stack electrodes in A/m^2 . α_{an} is the charge transfer coefficient of anode side. It is calculated experimentally in [18] to be 0.7353.

$$V_{act} = \frac{R \cdot T_{op}}{2 \cdot \alpha_{an} \cdot F} \cdot \operatorname{asinh} \left(\frac{i_{dens}}{2 \cdot i_{0,an}} \right) \quad [V] \quad (3.4)$$

Ohmic overpotential, V_{ohm} , is the energy loss due to resistance of membrane in cell and it is dominated at medium current densities. Ohmic overpotential is calculated simply by Ohm's Law as shown in equation 3.5. Here, $R_{mem}[\Omega m^2]$ is the membrane resistance, calculated from membrane conductivity $\sigma_{mem}[S/m]$ and membrane thickness $\delta_{mem}[m]$. Nafion 117 membrane, with a δ_{mem} of 178e-6m. Temperature dependence of membrane conductivity can be modelled using Arrhenius expression [20] in equation 3.7. The values for E_{pro} , activation energy required for the proton transport in membrane, and $\sigma_{mem,std}$, membrane conductivity at the reference temperature and pressure conditions are experimentally calculated in [18].

$$V_{ohm} = R_{mem} \cdot i_{dens} \quad [V] \quad (3.5)$$

$$R_{mem} = \frac{1}{\sigma_{mem}} \delta_{mem} \quad (3.6)$$

$$\sigma_{mem} = \sigma_{mem,std} \cdot \exp \left(\frac{E_{pro}}{R} \cdot \left(\frac{1}{T_{op}} - \frac{1}{T_{std}} \right) \right) \quad (3.7)$$

Additionally, concentration (diffusion) overpotential occurs when electrolysis reaction is fast and the mass transport is relatively slow. Its effect is dominant at high current densities. Concentration overpotential is ignored in this model assuming nominal cell current never reaches high current densities that concentration overpotential is dominant.

Electrolyser cell current and active power consumption is calculated using equations 3.8-3.9. $A_{membrane}$ in equation 3.8 is membrane area in cm^2 , which is 290. Nominal power of 60 electrolyser cells is considered

to be 46 kW according to empirical parameters from [18] and these outputs are scaled according to 50 MW capacity of electrolyser.

$$I_{cell} = A_{membrane} \cdot i_{dens} \quad [A] \quad (3.8)$$

$$P_{cell} = I_{cell} \cdot V_{cell} \quad [W] \quad (3.9)$$

Input of pressure submodel is stack operation temperature T_{op} and the output is the partial pressures of water, hydrogen and oxygen as described in equations 3.10-3.12. Partial pressure of water, pp_{H2O} , is calculated using the empirical equation from [18]. The hydrogen and oxygen partial pressures are calculated using Dalton's law of partial pressures as shown in equations 3.11 - 3.12.

Pressure:

$$pp_{H2O} = 6.1078 \cdot 10^{-3} \cdot \exp\left(17.2694 \cdot \frac{T_{op} - 273.15}{T_{op} - 34.85}\right) \quad [bar] \quad (3.10)$$

$$pp_{H_2} = p_{cat} - pp_{H2O} \quad [bar] \quad (3.11)$$

$$pp_{O_2} = p_{an} - pp_{H2O} \quad [bar] \quad (3.12)$$

Massflow sub-model describes the mass transfer phenomena occurring in electrolysis cell with equations 3.13 - 3.15. The input of this submodel is cell current calculated in electrochemical sub-model. η_f is the faraday efficiency assumed to be 1. n_{cells} is the number of electrolyser cells, which is 60 per stack.

Massflow:

$$\dot{n}_{H_2} = \frac{n_{cells} \cdot I}{2 \cdot F} \cdot \eta_f \quad [mol/s] \quad (3.13)$$

$$\dot{n}_{O_2} = \frac{n_{cells} \cdot I}{4 \cdot F} \cdot \eta_f \quad [mol/s] \quad (3.14)$$

$$\dot{n}_{H_2O} = \frac{n_{cells} \cdot I}{2 \cdot F} \cdot \eta_f \quad [mol/s] \quad (3.15)$$

Electrochemical, pressure and massflow sub-models are same for both model. However, for model B, thermal domain is also created with lumped thermal capacitance model. Temperature of the electrolyser system is simplified with one equation 3.16. The first term on the right side is for heat generated by electrolysis reaction and it depends on cell voltage and current, as shown in equation 3.17. $V_{tn} = 1.48V$ is the thermo-neutral voltage of electrolysis in [18]. Second one for the work contribution of circulation pump, as in equation 3.18. Here, rated electric power consumption of the pump, $W_{pump,elec}$, is 1100W, and the pump efficiency, $\eta_{motor,elec}$, is 0.75. Third one for the heat removed by cooling system, it has linear relation with the consumed active power and offset base power. Fourth one is for the heat lost to ambient it depends on operation and ambient temperature. R_{th} is experimentally calculated thermal resistivity of electrolyser. The last term comes from enthalpy lost with the products leaving the system, it has empirical equation that depends on temperature [61]. Considering equations (3.1 - 3.15) adding this dynamic sub-model, equation 3.16, to the system makes the general behavior of the electrolyser dynamic, since each sub-model depends on temperature parameter directly or indirectly.

Thermal:

$$C_{th} \frac{dT}{dt} = \dot{Q}_{elec, heat}(V, I) + \dot{W}_{pump, loss}(P) - \dot{Q}_{cooling}(P) - \dot{Q}_{loss}(T) - \sum_j \dot{n}_j \cdot \Delta h_j \quad (3.16)$$

$$\dot{Q}_{elec, heat} = (V_{cell} - V_{tn}) \cdot I \cdot n_{cells} \quad (3.17)$$

$$\dot{W}_{pump, loss} = \dot{W}_{pump, elec} \cdot \eta_{motor, elec} \quad (3.18)$$

$$\dot{Q}_{loss}(T) = \frac{1}{R_{th}} (T_{op} - T_{amb}) \quad (3.19)$$

Table 3.1 summarizes the features of electrolyser models. Model "A", operates at constant temperature 60 °C while Model "B" calculates the temperature of the electrolyser system with dynamic thermal submodel. Both models are semi-empirical and have static equations but thermal submodel is dynamic which makes the general behaviour of the electrolyser system dynamic for Model "B". Finally, thermal submodel equation also includes balance of plant (BOP) elements such as circulation pump or cooling work that affect the temperature evolution and efficiency of electrolyser. Figure 3.2 illustrates created electrolyser models.

Table 3.1: Modelling considerations of electrolyser

Model	Physical Domains	Modelling Approach	Dynamic Behaviour	Modelling Scale
A	Electrochemical Electrical	Analytic + Empirical	Static	Cell/Stack
B	Electrochemical Electrical Thermal	Analytic + Empirical	Static + Dynamic (ODE)	Cell/Stack + BOP

Compressed Gas Storage Tank

Occupied storage capacity is modelled with equation 3.20. Storage volume V is assumed to be 100 m^3 . $H_{2,prod}$ is the amount of hydrogen in m^3 produced by electrolyser, as described in equation 3.21 and $H_{2,demand}$ is the scheduled industrial hydrogen demand profile described in section 2.4. Storage is assumed to be at constant temperature 80 °C with no loss. Units are converted to m^3 using the values in table 3.2.

$$S_{PtG} = \frac{\int (H_{2,prod} - H_{2,demand}) dt}{V} \quad [\%] \quad (3.20)$$

$$H_{2,prod} = n_{cells} \frac{M_{H_2}}{\rho_{H_2}} \cdot \frac{I_{cell}}{2 \cdot F} \cdot \eta_f \quad [m^3] \quad (3.21)$$

$$O_{2,prod} = n_{cells} \frac{M_{H_2}}{\rho_{H_2}} \cdot \frac{I_{cell}}{4 \cdot F} \cdot \eta_f \quad [m^3] \quad (3.22)$$

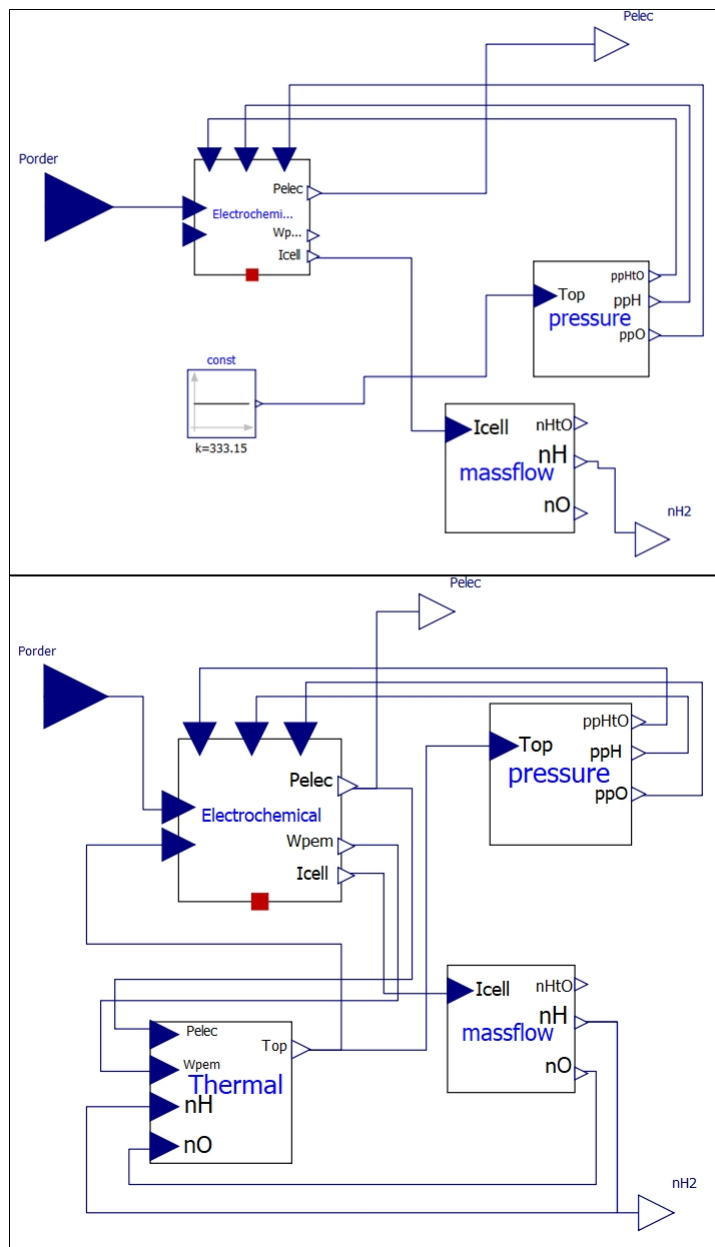


Figure 3.2: Electrolyser model "A" (upper) and model "B" (lower) model in OM

Table 3.2: Hydrogen & Oxygen characteristics at 80 °C

Parameter	Hydrogen	Oxygen
M (molar mass) [kg/mol]	2.016e-3	31.999e-3
ρ (density) [kg/m³]	0.06953	1.104
F (faraday constant)	96485	96485

Adjustable Power Level Controller

Figure 3.3 illustrates the implemented controller model in OM. In a normal operation where there is available space in the storage, minimum active power is controlled such that scheduled energy demand is always balanced by generation. However, when there is no available space in the storage, PtX is forced to work under 10% load until storage energy level is lower than maximum. When the storage energy level is below emergency level, which is assumed to be 50%, PtX is forced to work at nominal power until it reaches normal operation conditions. Maximum active power value is nominal power during normal operation, however it

strictly follows minimum active power if storage is in another state.

$$P_{min} = \begin{cases} 0.1 \text{ p.u.} & \text{if } S_{storage}(t) > S_{max} \\ P(t) - (\dot{n}_{H_2,prod} - \dot{n}_{H_2,demand}) \times K_{gain} & \text{if } S_{emergency} \leq S_{storage}(t) \leq S_{max} \\ 1.0 \text{ p.u.} & \text{if } S_{storage}(t) < S_{emergency} \end{cases}$$

$$P_{max} = \begin{cases} 1.0 \text{ p.u.} & \text{if } S_{emergency} \leq S_{storage}(t) \leq S_{max} \\ P_{min} & \text{else} \end{cases}$$

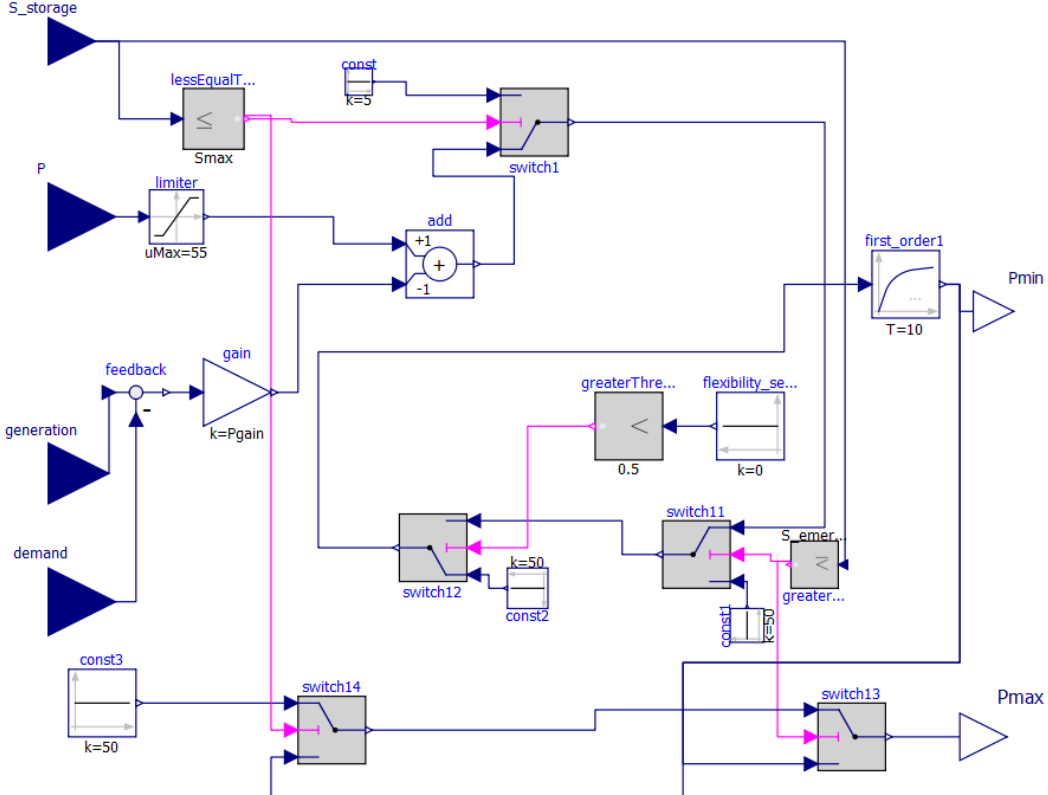


Figure 3.3: Adjustable power level controller in OM

Static Generator

Static generator models in figure 3.1, 3.4 are directly from iPSL library [59]. Their behaviour is similar to current-controlled voltage source converter, and they provide interface with the electrical network.

3.1.2. Power-to-Heat

Figure 3.4 shows created power-to-heat model. The inputs of the model are scheduled district heat demand that defines minimum active power of heat pump and ambient temperature. In addition to these, active power set points to control heat output and/or voltage set point for reactive power control can be used. Details of heat pump and hot water storage tank model are explained below. Adjustable power level controller and static generator models are similar to power-to-gas.

Heat Pump

COP of a heat pump depends on the choice of refrigerant and the rankine cycle efficiency (Carnot efficiency) of that refrigerant inside the heat pump as described in equation 3.23. Using pressure - enthalpy table of refrigerant R134a and Matlab curve fitting tool, fifth order polynomial functions of COP depending on ambient and condenser temperatures are created. In figure 3.5, enthalpy at state 1 and state 3, depends on inlet and outlet temperatures and already known from saturated vapor and liquid table af R134a, see appendix D.

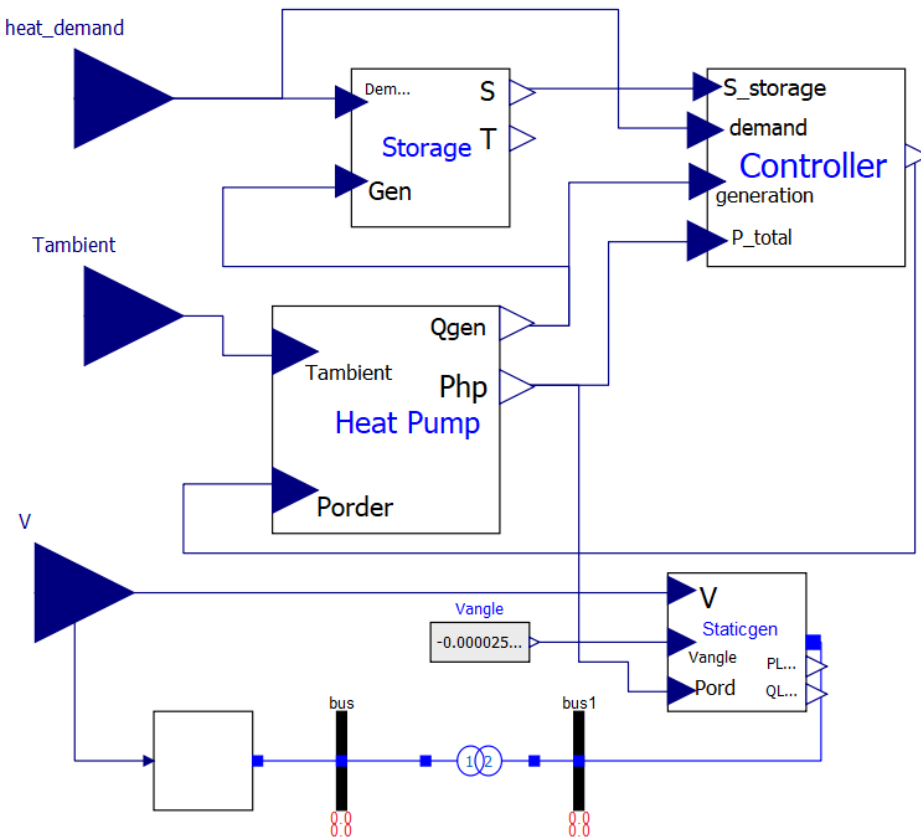
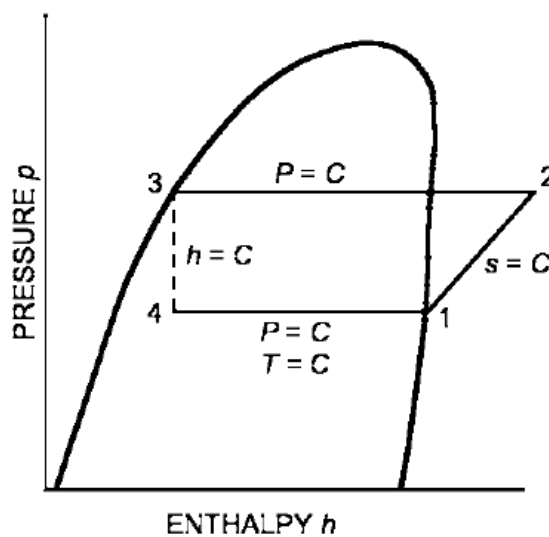


Figure 3.4: Power-to-heat model in OM

Enthalpy at point two, h_2 , calculated by linear interpolation of the super-heat tables for R-134a assuming isentropic compressor work. Rest of the assumptions described in figure 3.5. As a result COP values are calculated for various $T_{ambient}$ and $T_{condenser} = 50, 70^{\circ}\text{C}$ conditions as given in table 3.3 and these results are used to create fifth order polynomial function of COP that depends on ambient and output temperatures.

Figure 3.5: Theoretical Single-Stage Vapor Compression Refrigeration Cycle ($C = \text{Constant}$) [16]

$$COP = \frac{Q_{produced}}{P_{consumed}} = \frac{Q_{condenser}}{W_{compressor}} = \frac{h_2 - h_3}{h_2 - h_1} \quad (3.23)$$

Table 3.3: COP results for various ambient and condenser temperatures

$T_{ambient}$	-20	-16	-12	-8	-4	0	4
COP @ $T_{cond} = 50^\circ C$	3.3931	3.6429	3.9268	4.2500	4.6251	5.0604	5.5750
COP @ $T_{cond} = 70^\circ C$	2.4174	2.5586	2.7150	2.8887	3.0837	3.3013	3.5476
$T_{ambient}$	8	12	16	20	24	28	32
COP @ $T_{cond} = 50^\circ C$	6.1957	6.9452	7.8660	9.0564	10.5899	12.7115	15.7889
COP @ $T_{cond} = 70^\circ C$	3.8298	4.1514	4.5195	4.9559	5.4618	6.0736	6.8178

Three different models are considered for power-to-heat as explained in table 3.4. In model A, daily average ambient temperature is considered to be the evaporator temperature and it is constant during the day. For model B & C, hourly measured ambient temperature is considered to be the inlet temperature of heat pump. Additionally, for model C, auxiliary electric boiler is connected to the output of electric heat pump in order to increase the efficiency of heat pump. Table 3.4 shows modelling considerations for heat pump.

Figure 2.5 illustrates the heating cycle of PtH. With a return temperature equal to ambient, water is pumped to the evaporator of the heat pump. Here assuming constant mass flow rate for circulation pump, the energy output of heat pump is defined by compressor work and coefficient of performance. Basic approach to model electric heat pump is assuming constant COP and no change in temperature. This approach is considered for model A and described with equation 3.24 in this project. However, in reality COP strongly depends on temperature levels of the energy source. Therefore, regression analysis is carried out in order to create a polynomial function of COP depending on the inlet and outlet temperatures. As a result, COP performance is modelled as shown in equation 3.25. Additionally, COP increases when temperature difference between the inlet and outlet of the heat pump decreases. Therefore, especially during winter when the weather is cold, heat pump capacity might need to be increased with an auxiliary electric boiler to increase heat pump efficiency. Therefore, for model C, when the ambient temperature is below 15 °C, electric boiler is activated, as explained in equations 3.26-3.28, in order to increase the efficiency and heat capacity.

Table 3.4: Modelling considerations of heat pump

Model	Modelling Approach	Ambient Temperature	Modelling Scale
A	Regression	Daily average	Heat pump
B	Regression	Hourly measured	Heat pump
C	Regression	Hourly measured	Heat pump with auxiliary electric boiler

Model A:

$$P_t = \frac{\dot{Q}_t^{HP}}{COP_{average}} \quad \forall t \quad (3.24)$$

Model B & C:

$$P_t = \frac{\dot{Q}_t^{HP}}{COP_t^{real}(T_{inlet}, T_{outlet})} \quad \forall t \quad (3.25)$$

For Model C:

if $T_{amb} \leq 15^\circ C$:

$$Q_{boiler} = \dot{m}c\Delta T \quad (3.26)$$

$$\eta_{boiler} = 99\% \quad (3.27)$$

$$P_{boiler} = \frac{Q_{boiler}}{\eta_{boiler}} \quad (3.28)$$

Fifth order polynomial function of COP is shown in equation 3.29. Matlab curve fitting results are shown in figure 3.6, 3.7 and calculated coefficient results of fifth order polynomial function is shown in table 3.5. Two different COP equation coefficients are created for $T_{condenser} = 50$ and $70^\circ C$. This is because, for model C, when the ambient temperature drops below $15^\circ C$, heat pump output temperature is switched to $50^\circ C$ to increase heat pump efficiency and the rest of the energy is supplied by electric boiler in order to increase supply temperature to $70^\circ C$.

$$COP(T_{amb}) = a_1 T_{amb}^5 + a_2 T_{amb}^4 + a_3 T_{amb}^3 + a_4 T_{amb}^2 + a_5 T_{amb} + a_6 \quad (3.29)$$

Table 3.5: 5th order polynomial fuction parameters for $T_{condenser} = 50, 70^\circ C$

$T_{condenser} (\text{ }^\circ\text{C})$	a_1	a_2	a_3	a_4	a_5	a_6
50	3.46e-8	1.29e-6	4.35e-5	2.387e-3	1.186e-1	5.063
70	1.46e-8	-9.66e-8	6.61e-6	1.01e-3	5.864e-2	3.295

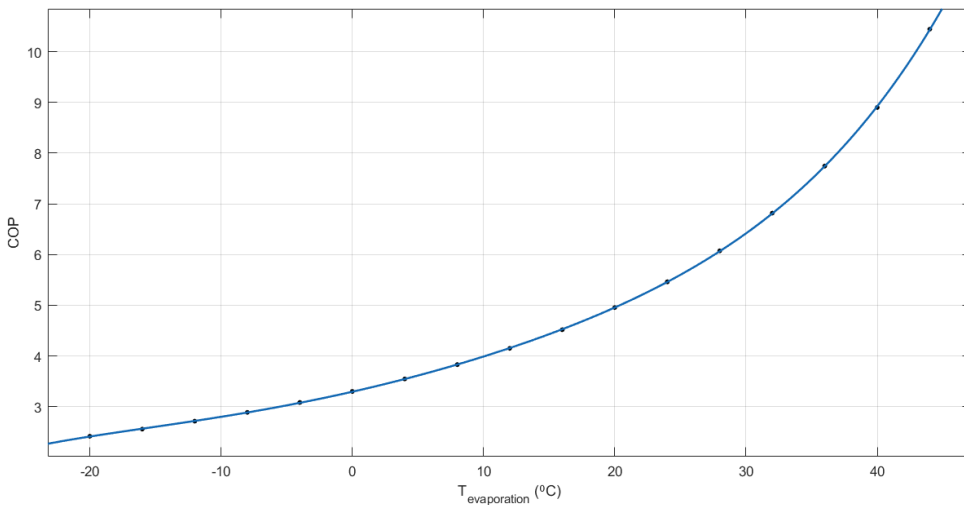
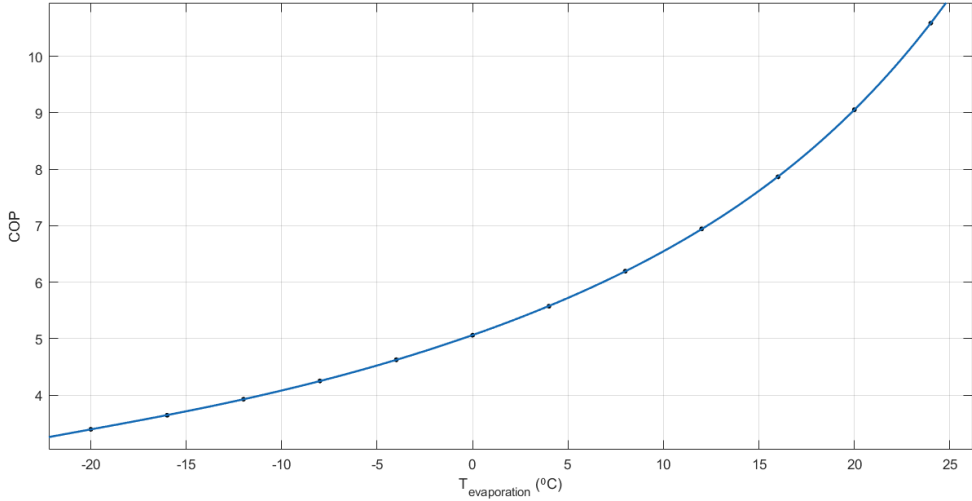


Figure 3.6: COP vs. $T_{ambient}$, $T_{condenser} = 70^\circ C$

Figure 3.7: COP vs. $T_{ambient}$, $T_{condenser} = 50^\circ\text{C}$

Hot Water Storage Tank

Occupied storage capacity is modelled with equation 3.30. Storage volume V is assumed to be 2400 m^3 . Q_{prod} is the amount of heat energy in m^3/s produced by heat pump, It is converted to from kg/s to m^3/s as described in equation 3.31, using specific heat and density of water at 70°C . Values of equation 3.31 is given in table 3.6. Q_{demand} is the scheduled district heating demand profile described in section 2.4.

$$S_{PtH} = \frac{\int(Q_{prod} - Q_{demand})dt}{V} [\%] \quad (3.30)$$

$$\dot{m} Q_{prod,[\text{kJ/kg}]} = c_p \rho (70 - T_{amb}) Q_{prod,[\text{m}^3/\text{s}]} \quad (3.31)$$

Table 3.6: Power-to-Heat storage parameters

Parameter	Value
\dot{m} (massflow) [kg/s]	5
Q [kJ/kg] (t)	
c_p (specific heat) [$\text{kJ}/(\text{K kg})$]	4.190
ρ (density) [kg/m^3]	977.74
Storage Volume [m^3]	2400

3.1.3. Electrical Base Load

20MW constant electrical base load connected in PandaPower, as illustrated in figure 2.1, to represent the constant base load in the industrial area.

3.2. Renewable Energy Sources

Renewables.ninja [48] models are used. Renewables.ninja allows user to run simulations of the hourly power output from wind and solar power plants located anywhere in the world. Wind farm model as described in [54] and PV farm model as described in [49]. For hourly output of RES, see appendix B.

3.3. Electrical Network & Optimal Power Flow

Figure 3.8 illustrates the co-simulation flowchart. Red dashed line, CEMS, represents the higher control level that is Pandapower and blue dashed line represents, lower control level, that is MES agents. At $t = 0$, optimal

power flow (OPF) solver in pandapower calculates the optimum operation point with the objective of minimizing operational cost. After that the results of the OPF are sent to MES agents. Here PtX models simulate until the next exchange time and send out the adjustable power level and cost binding information to higher control level for the next calculations.

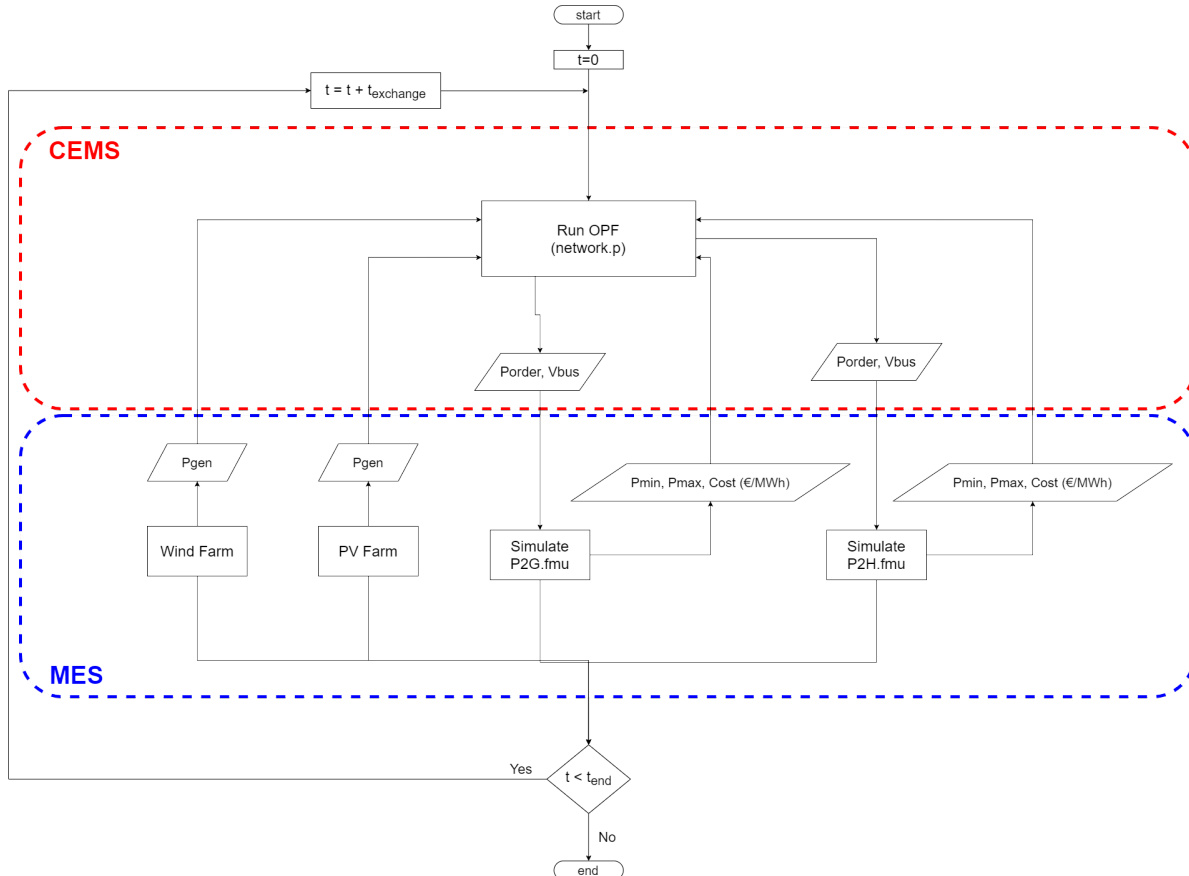


Figure 3.8: Co-simulation flow chart

3.3.1. Formulation of the Optimization Problem

Python-based tool Pandapower is used for the energy management of MES. Pandapower optimal power flow solver has objective function to minimize operational cost, as shown in equation 3.32. Linear cost signals are calculated depending on the efficiency of device in Modelica, as explained in section 2.4 and sent to pandapower as the c_1 value of the polynomial cost function in equation 3.33.

Objective function:

$$\min \sum_{i \in \text{load}} f_i(P_i) \quad (3.32)$$

Cost function:

$$f_{pol}(p) = c_n p^n + \dots + c_1 p + c_0 \quad (3.33)$$

Optimal power flow problem of pandapower considers the constraints shown in table 3.7. Bus constraint contains maximum and minimum voltage magnitude, branch constraints contain maximum loading percentage and, attention of this project, operational power constraints contains the active and reactive power generation of generators or loads as operational flexibility for the OPF. This means, higher control level which is pandapower has to communicate with modelica agents and learn the adjustable power level, which is P_{min} and P_{max} , in order to calculate the optimum operating point within this range. Optimal power flow solver

calculates the exact operation point for the next time step considering cost signals within the available range defined by the physical situation of the agents. Thus, existing OPF problem of Pandapower is enhanced by adding OM agents and controlling these boundaries depending on the storage situation of agents.

Table 3.7: Constraints

Element	Constraint	Remarks
Load Static Generator External Grid	$P_{min,i} \leq P_i \leq P_{max,i}$ $Q_{min,i} \leq Q_i \leq Q_{max,i}$	Operational power constraints (Device flexibility)
Transformer	$L_i \leq L_{max,i}$	Branch constraint (maximum loading percentage)
Line	$L_i \leq L_{max,i}$	Branch constraint (maximum loading percentage)
Bus	$V_{min,i} \leq V_i \leq V_{max,i}$	Network constraint

3.4. Co-simulation Setup

Co-simulation inputs and outputs can be seen in figure 3.8. Python-based tool Energysim is used to combine Modelica FMU's for PtX agents and Pandapower pickle file for optimal power flow; and implement this complex simulation in a relatively simple way by only using necessary i/o. Figure 3.9 shows the macro step time that optimal power flow solver and Modelica agents exchange information, and micro step time that the agents simulate. With the considered exchange time and duration, simulation takes approximately 8 min.

- Simulation duration: $3600 * 24 (s)$
- Exchange time: 900 (s)
- Step time P2G: 3 (s)
- Step time P2H: 3 (s)
- Step time OPF: 300 (s)

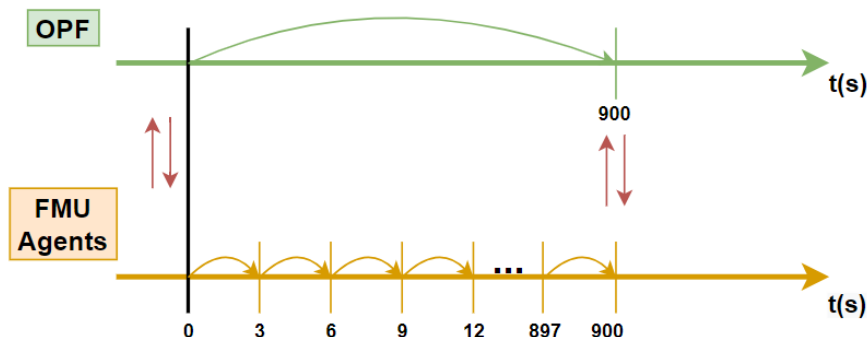


Figure 3.9: Co-simulation synchronization

4

Results & Discussions

4.1. Model Validation

PEM electrolyser model and COP of heat pump with refrigerant R134a is validated in this section comparing with references.

4.1.1. PEM electrolyser model validation

Electrolyser cell voltage response to varying cell current densities is compared with the reference model [18] in figure 4.1. Experimentally measured voltage response above is from the reference paper and the curve below is the modelled electrolyser's cell voltage response. It is observed that maximum error is not smaller 0.1 V. Thus, the electrolyser cell characteristic matches with the reference model [18] and model is validated.

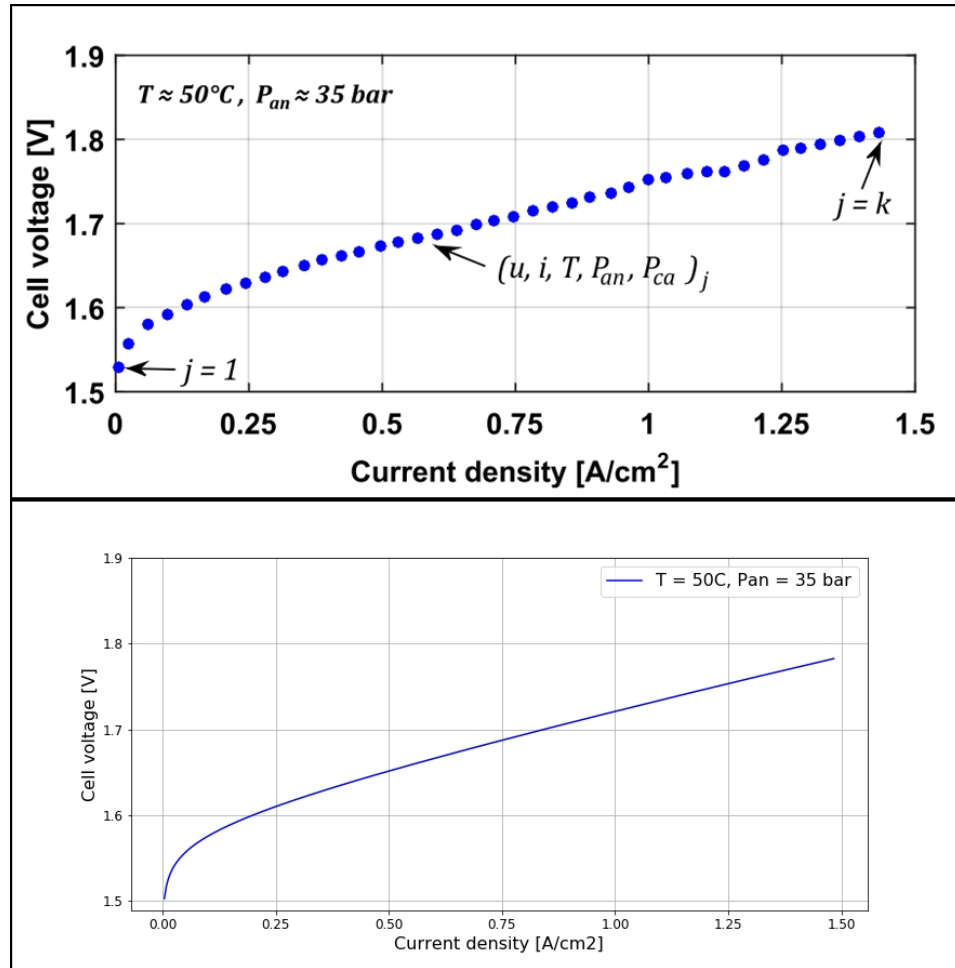
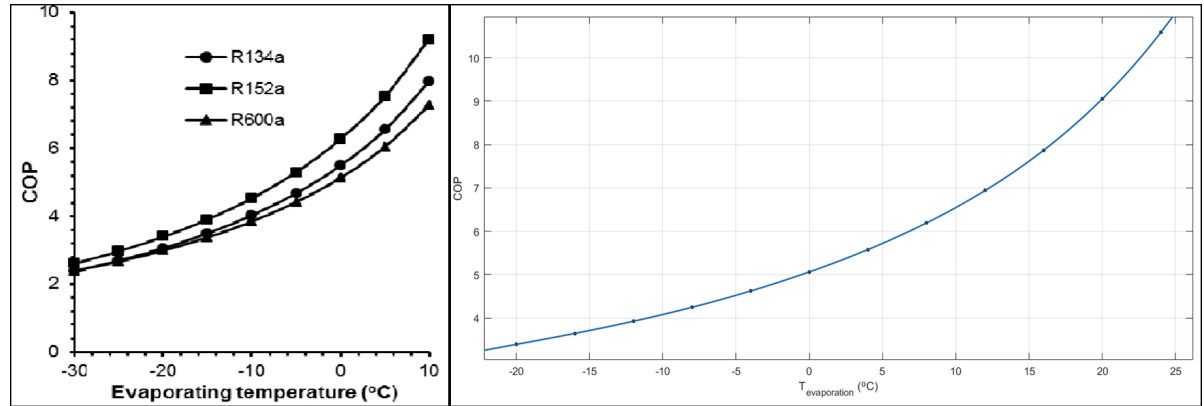


Figure 4.1: PEM Electrolyser cell voltage vs. current density

4.1.2. Heat pump model validation

COP of refrigerant R134a with respect to varying evaporator temperature and $T_{condenser} = 50^\circ\text{C}$ from reference [12] is compared with the curve fitting result of COP for $T_{condenser} = 50^\circ\text{C}$. It can be observed that maximum error is approximately 0.2 between models. This error is considered to be small enough to ignore. It is mostly due to pressure approximations made from superheat vapor table of R134a.

Figure 4.2: Coefficient of performance (COP) vs. evaporating temperature for $T_{cond} = 50^\circ\text{C}$

4.2. Analysis

Implementation of analysis is explained in section 2.5 and results are shown below.

4.2.1. Multi-Energy System Analysis

MES analysis is carried out in order to understand the flexible capacity of considered power system. Figure 4.3 illustrates the wind and solar farm capacity in the area.

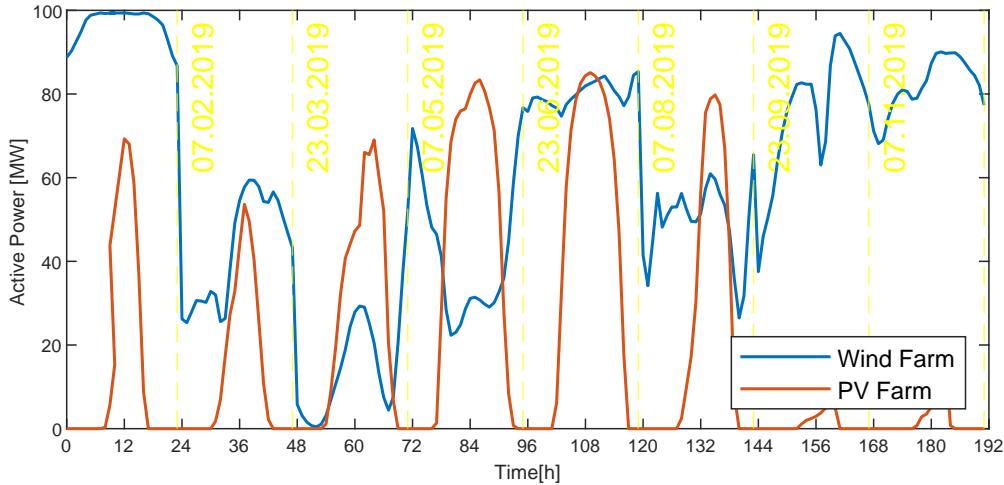


Figure 4.3: Power capacity of renewable energy sources

Figure 4.4 shows the flexible capacity in the area. Blue line is the sum of the power output of WF and PV farm and red line is the sum of active power consumption of model B of each PtX. 8 vertical dashed lines are illustrated in the following figures to separate each day easily. It can be observed that, in this area energy can be stored during summer season and this stored energy can be used during winter or spring time. Longer sun hours during summer not only increases the magnitude of excess RE but also increases the duration of Excess RE time. Thus, summer season provides opportunity for longer flexibility services. Extreme wind conditions during winter can also provide opportunity for shifting demand. But it should be considered for shorter flexibility services due to smaller time duration of excess RE. Thus, according to this figure 07.02.2019 is selected for 24 hour simulations in power system analysis.

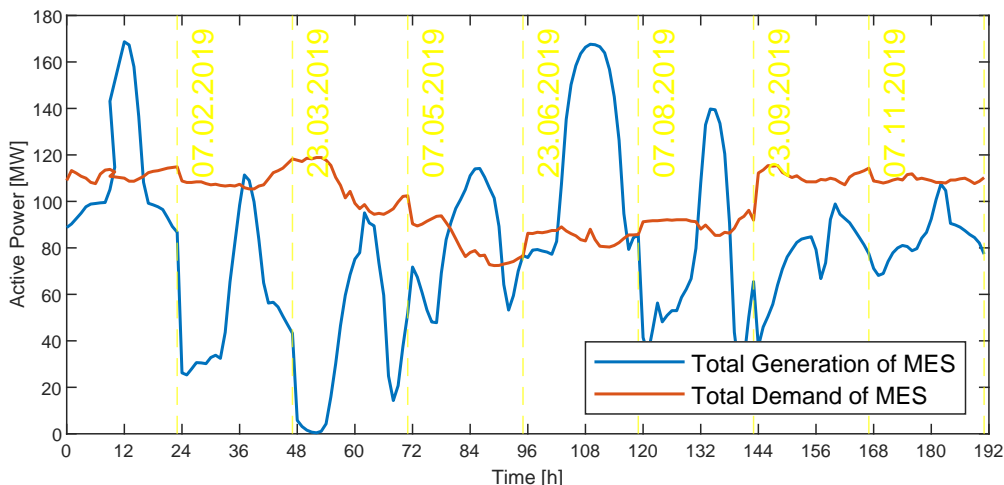


Figure 4.4: Flexible demand of multi-energy system

4.2.2. Power-to-X Model Comparison

PtX model analysis is implemented in order to investigate temperature evolution of models and their efficiencies for the same energy demand profiles. The effects of temperature evaluations on efficiency curves can be observed in the figures 4.5, 4.8. For electrolyser model A temperature is constant at 60 °C and model B it varies between 52 to 65 °C as illustrated in figure 4.6. With respect to temperature deviation, maximum efficiency difference is 0.6% in figure 4.5 which is not very significant. However, thermal sub-model is necessary to analyse the required capacity of auxiliaries. If the cooling capacity of the system would assumed to be less than necessary, than this would lead to larger temperature differences; therefore, bigger variations in efficiency results.

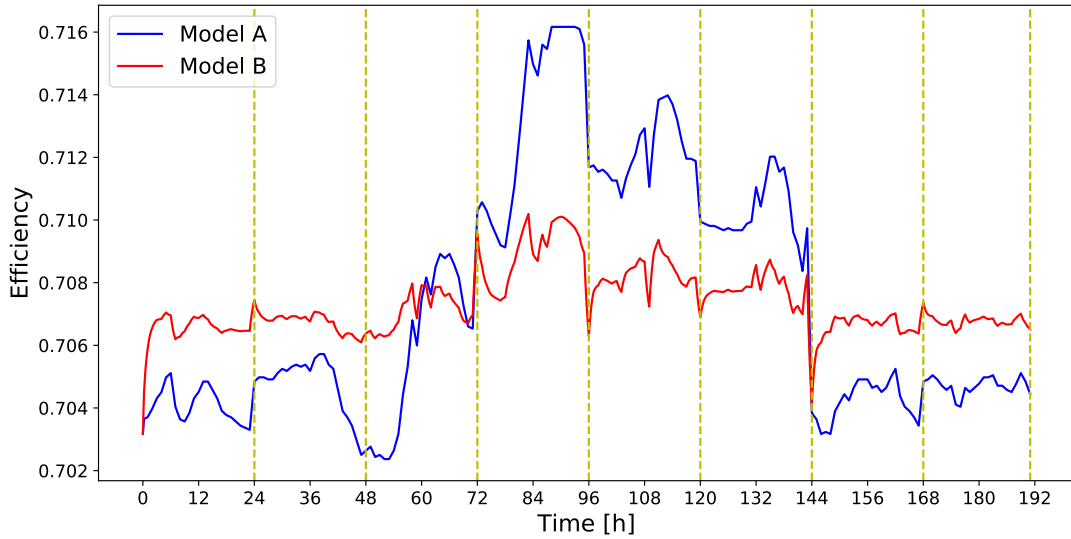


Figure 4.5: Efficiency comparison of electrolyser models vs. time

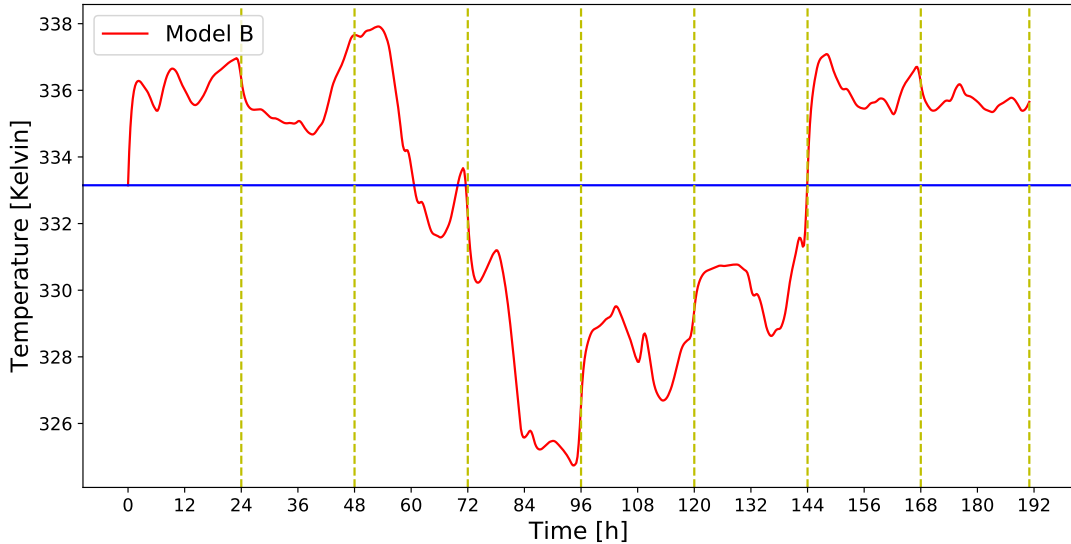
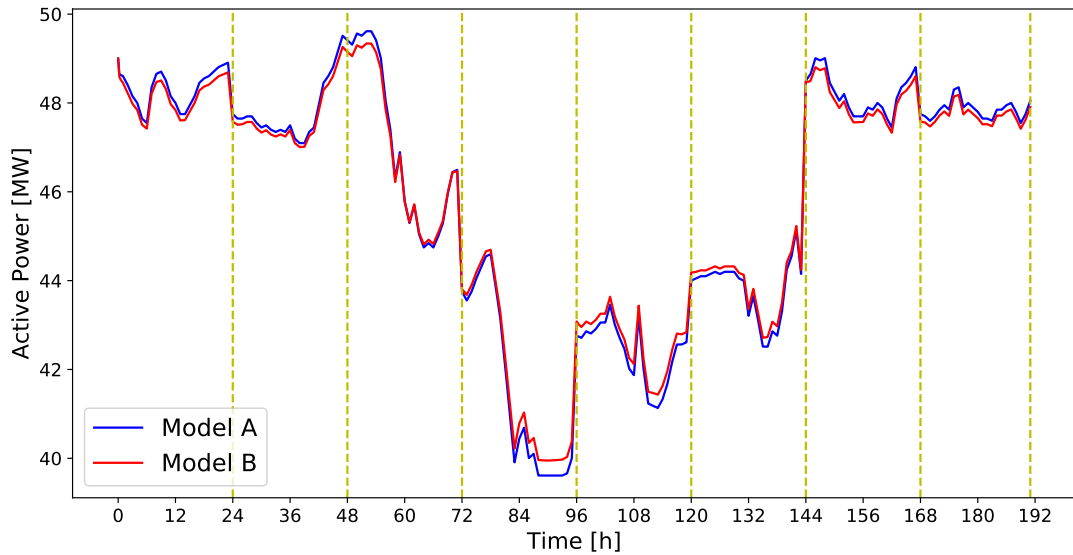


Figure 4.6: Operational temperature comparison of electrolyser models vs. time

Active power consumption of PtG models are compared in figures 4.7. Maximum power consumption difference between power to gas models is 0.4 MW for 50 MW electrolyser system. That corresponds to 0.8%, which is not very significant.

Figure 4.7: $P_{Load,PtG}$ of electrolyser models vs. time

Considered ambient temperatures shown in figure 4.9. For heat pump model A, COP is calculated from daily average temperature; therefore, it is constant during the day. For model B and C hourly measured temperature is used for COP calculations. Maximum COP difference between model A and B is 1.4 and model B and C is 3 in figure 4.8. Results show that temperature considerations have significant effect on COP characterization of heat pump and auxiliary boilers are able to improve efficiency of a heat pump considerably.

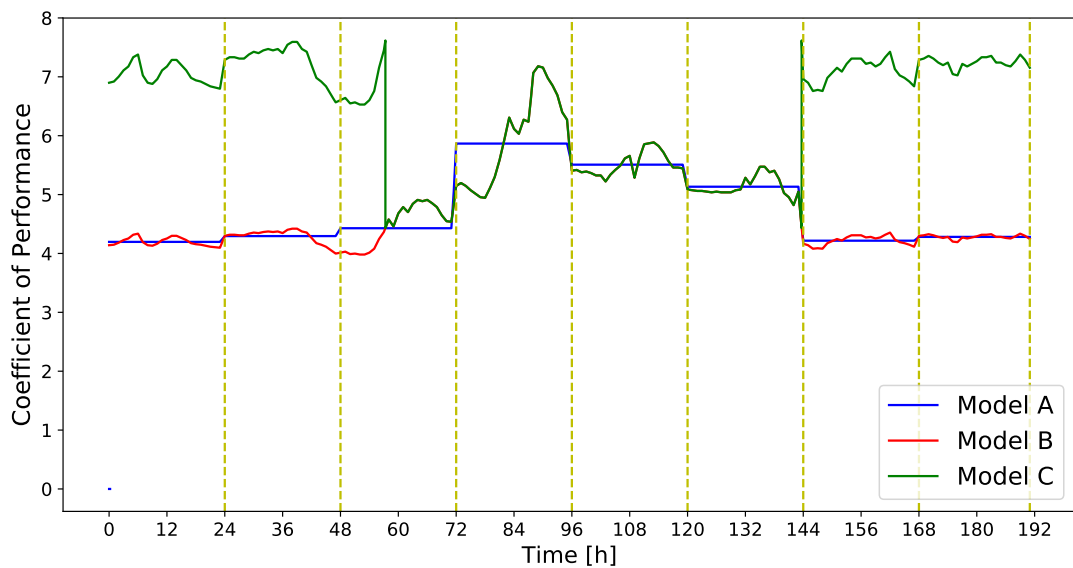


Figure 4.8: COP results of heat pump models vs. time

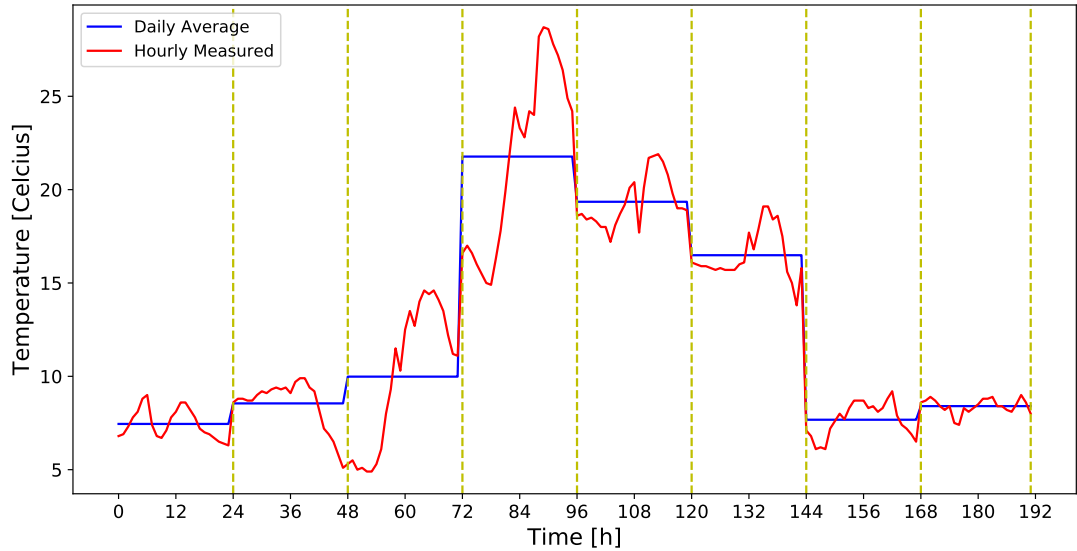


Figure 4.9: Ambient temperature vs. time

Active power consumption of PtH models are compared in figures 4.10. Maximum power consumption difference between power-to-heat model A and B is 9 MW and model B and C is 4.55 MW. This means 18% and 9% maximum error for 50 MW electric heat pump system, which is significant. Therefore, COP of a heat pump can be assumed constant if inlet and outlet temperatures remain stable during operation. Otherwise, COP must be calculated with respect to temperature levels of the energy source.

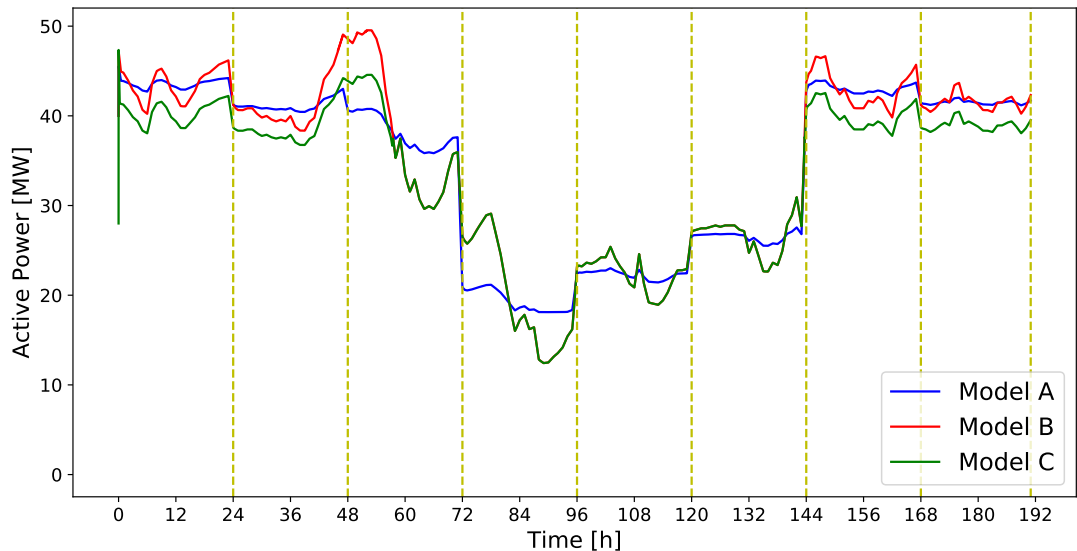
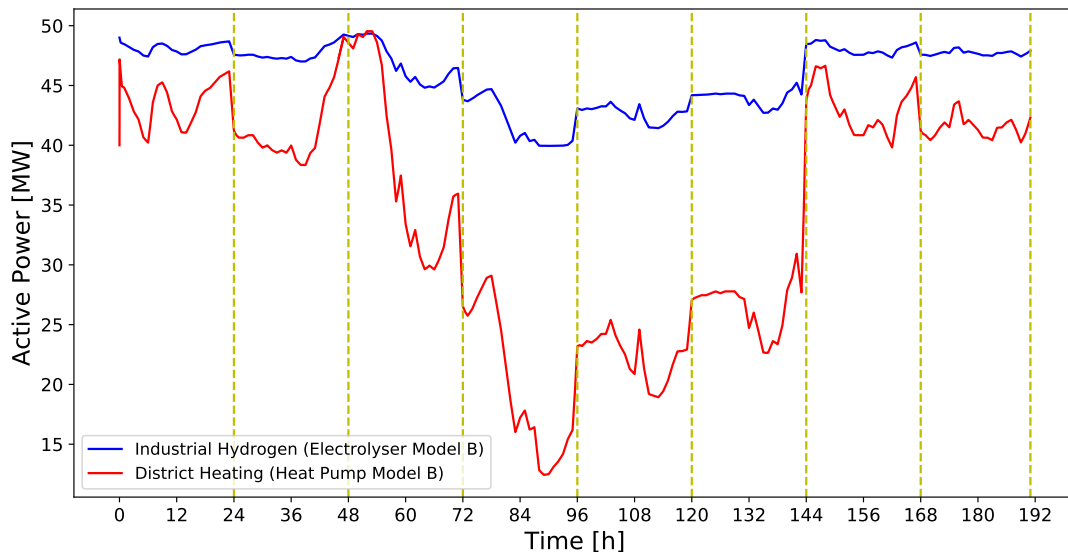
Figure 4.10: $P_{Load,PtH}$ of heat pump models vs. time

Figure 4.11 shows the demand curves of model B of each PtX. It is observed that industrial hydrogen demand has less variations with respect to changing ambient temperature than district heating demand as expected from section 2.4.

Figure 4.11: P_{Load} results for Model "B" of PtG & PtH vs. time

4.2.3. Power System Analysis

Base Case

Figure 4.12 shows the flexible active power demand of MES for base case. In this case, flexible demand of MES varies between +25 to (-60) MW. Results show that a flexibility service to store excess RE can be applied between 10:00 to 16:00 in this day. According to this flexibility service, resulting flexible demand curves are calculated for the first case.

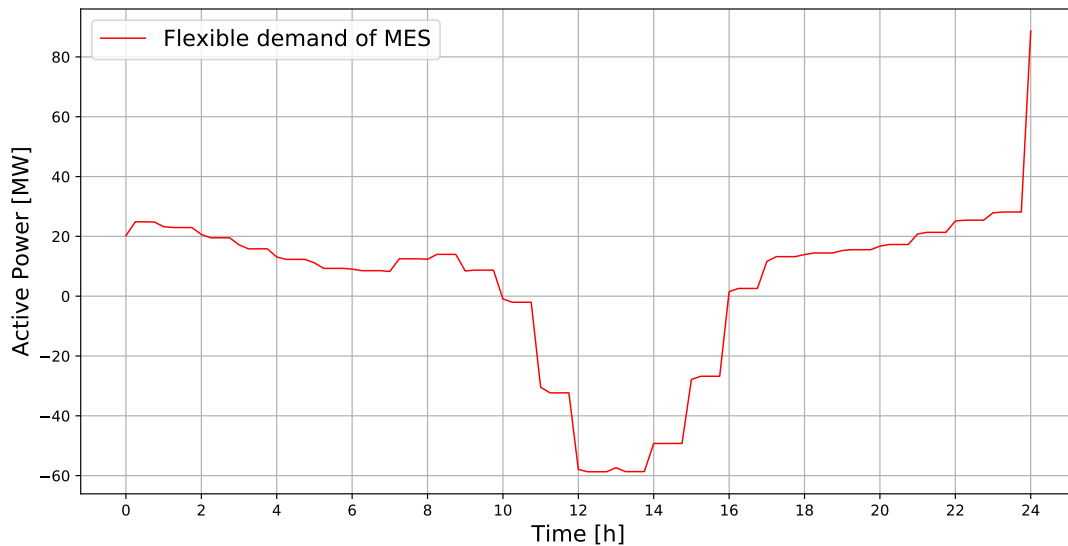


Figure 4.12: Flexible active power demand of MES on 07.02.2019 for base case

Case 1

Figure 4.13 compares the flexible demand of MES when only one of the PtXs is available for flexibility service. PtXs are controlled such that, during excess RE, available capacity is used to store this energy. Green line is the same curve in figure 4.12. Blue line is the active power consumption of PtG model B when only PtG is available for flexibility service in MES, and red line is the active power consumption of PtH model B when only PtH is available for flexibility service. As can be seen from figure 4.13, during excess RE, active power set point of available PtX is controlled in order to reduce the amount of excess RE and used to flatten the flexible demand curve. Since industrial demand is more stable at values close to nominal, it offers less flexibility. Therefore the difference between base case and PtG case is small and around 2 MW. On the other hand, PtH

operates at lower demands due to higher rate of change of heat demand. Therefore, it able to provide more flexibility to MES. Maximum difference between the base case and PtH case is approximately 10 MW.

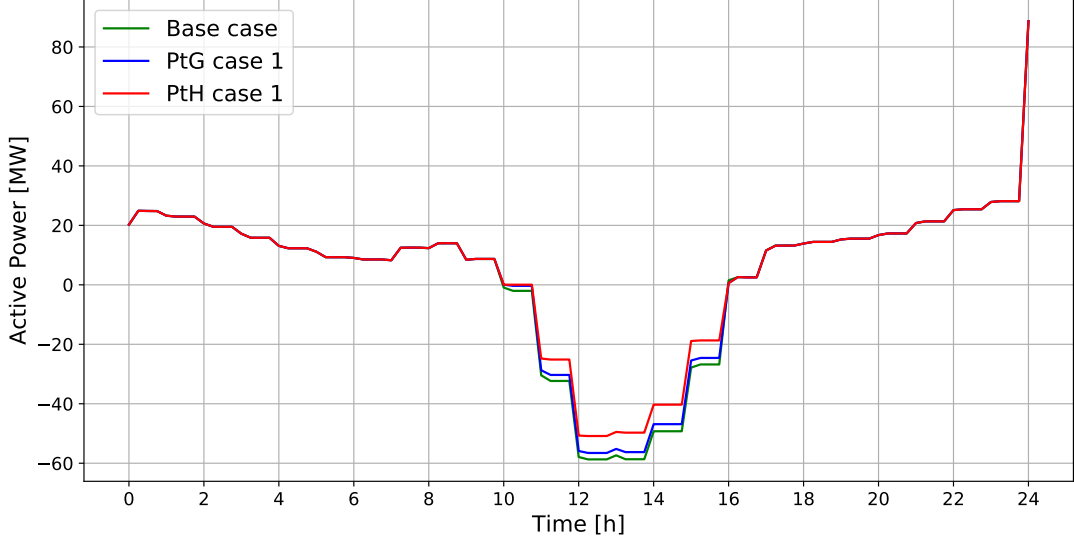


Figure 4.13: Flexible active power demand of MES on 07.02.2019 for case 1

Figure 4.14 compares the hydrogen production output of electrolyser models for the flexibility service in figure 4.13. Increasing hydrogen production due to excess RE can be observed between 10:00 to 16:00. Maximum difference between the hydrogen output of models is $0.032 \text{ m}^3/\text{s}$. For model B, exponential curve can be observed during flexibility service. Increasing power consumption, also increases the operational temperature of electrolyser. This new thermal equilibrium point for model B during excess RE, resulted with increasing hydrogen output during nominal active power order for electrolyser.

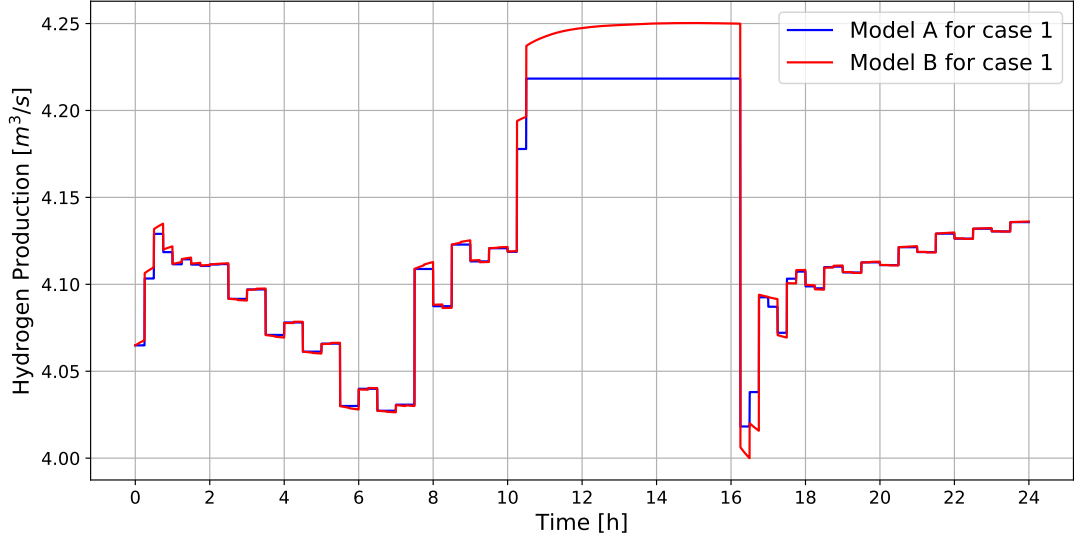


Figure 4.14: Hydrogen production of PtG models on 07.02.2019 for case 1

Figure 4.15 compares the heat production output of heat pump models for the flexibility service in figure 4.13. Green curve is for the heat pump with auxiliary electric boiler model. During 07.02.2019, ambient temperature is below 15°C ; therefore, auxiliary boiler is activated for model C. It is clear from the figure that auxiliary electric boiler increases the heat pump capacity significantly for heat pump, and it gives a great flexibility during excess RE. Maximum difference between model B and C is $0.96 \text{ m}^3/\text{s}$. Red curve is for model

B with hourly measured temperature input and the blue curve is for the model A with constant daily average temperature input. Maximum difference between model A and B is $0.20 \text{ m}^3/\text{s}$.

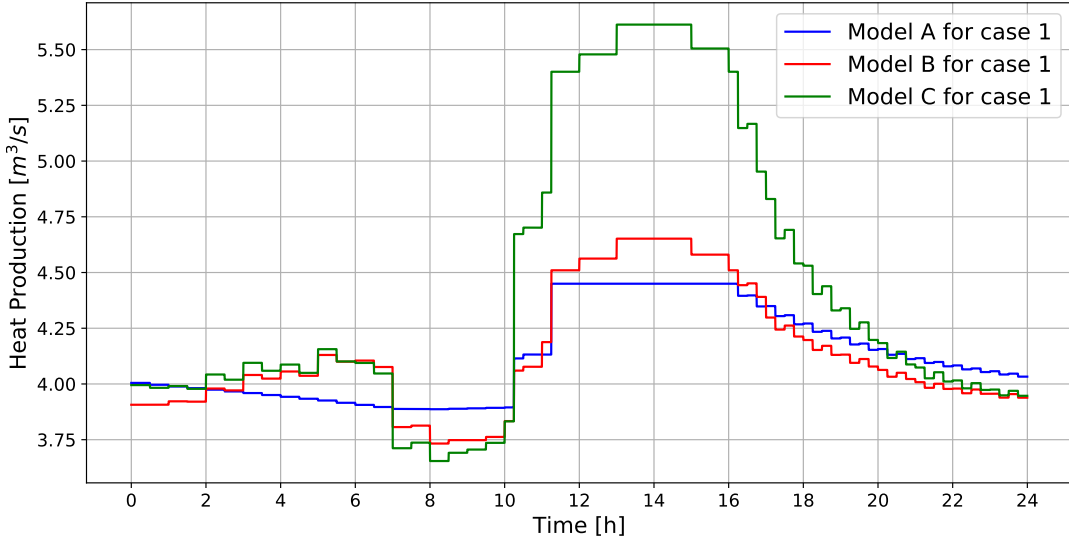


Figure 4.15: Heat production of PtH models on 07.02.2019 for case 1

Case 2

In this case, PtX load profiles explained in section 2.4 are lowered to half in order to observe the effects clearly. Figure 4.16 shows the leveled cost signals of PtG and PtH as explained in section 2.4. Figure 4.17 shows the resulting active power consumption of PtXs and the amount of excess RE. The effect of flexibility service from 10:00 to 16:00 can be observed in figure 4.17. During this time, active power consumption of PtX is increased in order to take the advantage of excess RE. In figure 4.17, flexibility of MES is able to compensate excess RE approximately for an hour from 10:00 to 11:00. However, after an hour the amount of excess RE is larger than the total capacity of available PtXs; therefore, excess RE starts to increase from approximately 11:00.

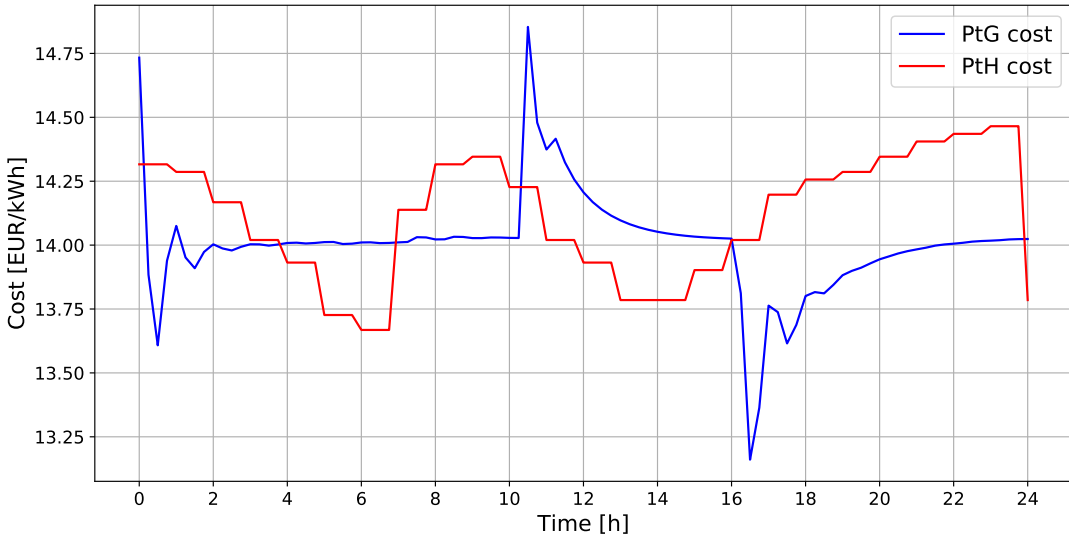


Figure 4.16: Leveled cost of PtX for case 2

The effect of cost signals on flexibility deployment can be observed between 10:00 to 11:00. Since the amount of excess RE is smaller than flexible capacity of PtX during 10:00 to 11:00, this excess energy needs to be optimally distributed between PtXs. As can be seen from figure 4.16, in the beginning of the flexibility service at 10:00, PtG cost is cheaper than PtH for approximately 30 minutes; therefore, PtG active power

consumption is set to nominal value 50 MW initially. However, after half an hour, PtH cost becomes cheaper than PtG cost for the rest of the flexibility service. This results with higher active power consumption of PtH than PtG after half an hour. This effect is observed in figure 4.17 from 10:00 to 11:00, as the blue line that represents the PtG load crosses the red line that represents the PtH load after 30 mins.

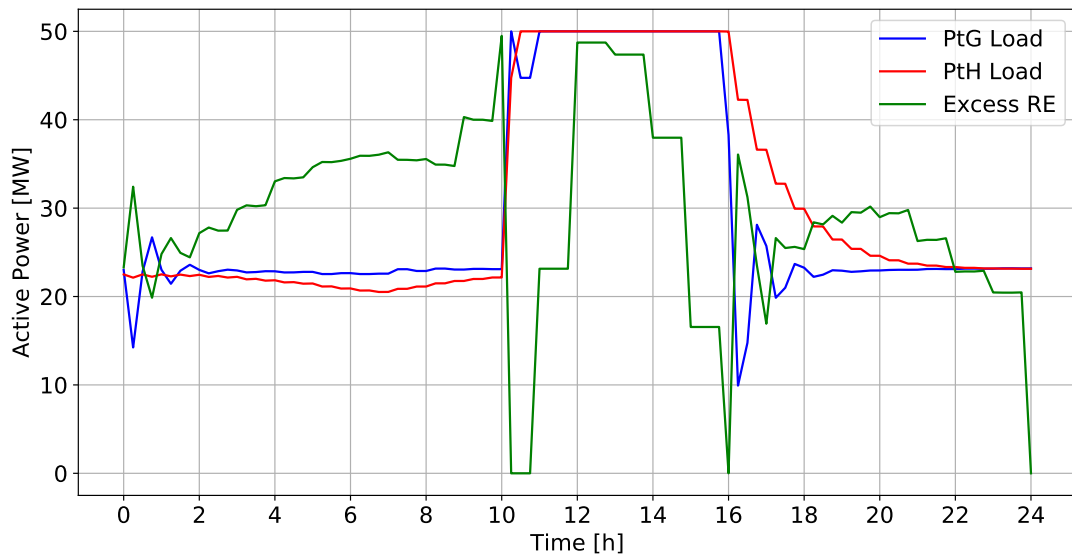


Figure 4.17: PtX active power consumption and Excess RE for case 2

5

Conclusion & Future Work

5.1. Conclusion

5.2. Recommendation for Future Work

A

Historical Data Processing & Probabilistic Weather

Historical data process is summarized in figure A.1. 2019 historical wind speed and solar irradiation data of RES location is divided into 8 regions that consists of 45 days. For every hour of each 45 day group a histogram table is created [22]. Then parameters of the Weibull and Beta PDF (shape, scale) are calculated by curve fitting in MATLAB using these tables.

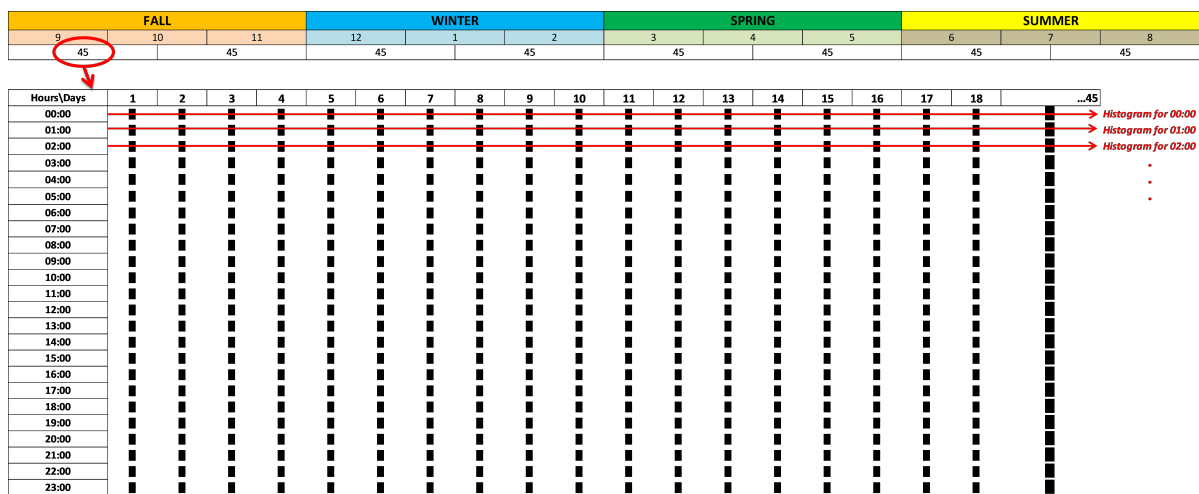


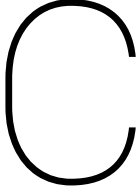
Figure A.1: Historical data processing

It was considered that probabilistic density function (PDF) of weibull and beta distribution for wind speed and solar irradiation generation, respectively, would be modelled based on historical data processing in order to investigate the effect of renewable energy generation models (Probabilistic vs. Historical data). However, it is observed that these models increase the simulation time significantly due to random generation of renewable energy sources with large amount of equations. Therefore, these models currently not in use and this part is excluded from the project.

B

Wind Farm & PV Farm Data

Hour\Day	7.02.2019			23.03.2019			7.05.2019			23.06.2019			7.08.2019			23.09.2019			7.11.2019			23.12.2019		
	Power (kW)	Speed (m/s)																						
0:00	88750.949	11.357	26222.646	6.026	5778.91	3.742	71760.561	9.325	75839.049	9.693	41444.907	7.124	37547.003	6.861	71138.664	9.271								
01:00	90293.251	11.659	25343.918	5.952	3129.872	3.145	67431.457	8.964	79043.579	10.029	34188.088	6.619	45931.625	7.431	68130.061	9.02								
02:00	92691.445	12.187	27907.221	6.161	1549.057	2.609	60889.148	8.451	79285.795	10.055	44850.676	7.359	50252.668	7.736	68972.071	9.089								
03:00	94943.193	12.897	30633.557	6.365	716.795	2.153	53278.167	7.929	78669.285	9.989	56283.77	8.138	55714.664	8.094	74136.082	9.539								
04:00	97679.965	14.228	30509.491	6.354	413.059	1.879	48115.306	7.575	78198.107	9.934	48165.889	7.577	64016.641	8.689	77557.683	9.896								
05:00	98850.022	15.322	30188.681	6.328	1095.603	2.39	46490.986	7.47	77243.433	9.838	50929.367	7.763	70894.933	9.245	79975.279	10.131								
06:00	99100.837	15.721	32822.538	6.529	3165.853	3.155	41149.653	7.102	76661.851	9.782	52996.879	7.91	76095.485	9.726	81036.2	10.253								
07:00	99382.052	16.694	31590.499	6.46	6867.586	3.937	28384.259	6.192	74697.25	9.591	52895.806	7.904	79305.323	10.057	80584.682	10.196								
08:00	99238.043	17.523	25590.066	5.971	10553.679	4.499	22338.246	5.702	77480.106	9.864	56227.548	8.134	82310.382	10.397	78760.55	9.998								
09:00	99349.675	17.157	26332.091	6.037	14436.677	4.951	23008.658	5.768	78786.739	10.001	52567.046	7.881	82674.717	10.451	78973.695	10.021								
10:00	99356.365	16.46	38080.872	6.89	18870.301	5.4	24853.248	5.921	79793.231	10.111	49573.244	7.668	82333.159	10.399	81306.589	10.284								
11:00	99333.389	16.334	49167.86	7.641	24356.035	5.88	28608.043	6.209	80934.875	10.241	49429.618	7.659	82348.441	10.406	83172.51	10.515								
12:00	99383.457	16.864	54587.354	8.017	27905.152	6.161	31151.452	6.407	81937.291	10.36	51394.572	7.802	76273.889	9.736	87300.527	11.106								
13:00	99278.348	17.416	57749.304	8.235	29307.875	6.265	31415.206	6.418	82505.947	10.429	57369.278	8.214	63028.409	8.624	89706.955	11.532								
14:00	99128.934	17.749	59427.451	8.357	29040.348	6.241	30777.014	6.371	83062.074	10.497	60948.575	8.47	68626.596	9.051	90078.552	11.616								
15:00	99122.275	17.76	59391.34	8.349	25193.696	5.945	29767.001	6.304	83750.64	10.59	59644.62	8.376	86850.573	11.038	89703.55	11.541								
16:00	99375.851	16.978	57832.151	8.249	20474.632	5.538	29044.578	6.247	84292.071	10.663	56074.862	8.117	93921.445	12.568	89807.618	11.561								
17:00	99195.918	15.915	54297.25	7.995	13290.124	4.832	30128.316	6.326	82669.919	10.445	53408.634	7.939	94476.638	12.737	89856.165	11.571								
18:00	98507.267	14.914	54086.295	7.983	7482.077	4.035	32681.769	6.519	80757.825	10.217	47225.525	7.512	92628.803	12.201	88915.665	11.39								
19:00	97685.474	14.232	56603.001	8.155	4246.706	3.456	35892.824	6.738	79381.122	10.066	35734.21	6.728	90811.928	11.767	87427.67	11.121								
20:00	96489.627	13.546	54587.368	8.017	7583.19	4.056	44830.193	7.349	77206.858	9.828	26468.626	6.045	87753.325	11.186	85747.873	10.864								
21:00	92980.903	12.297	50634.278	7.743	20709.728	5.559	58727.891	8.307	79324.886	10.059	31732.329	6.446	84581.58	10.703	84459.467	10.686								
22:00	89190.383	11.442	46900.932	7.489	37600.406	6.863	70017.108	9.168	84478.143	10.688	50210.49	7.721	81326.929	10.287	82105.607	10.375								
23:00	86740.936	11.014	43229.483	7.25	51959.945	7.835	76733.954	9.789	85345.637	10.811	65482.238	8.802	77500.611	9.866	77335.324	9.85								



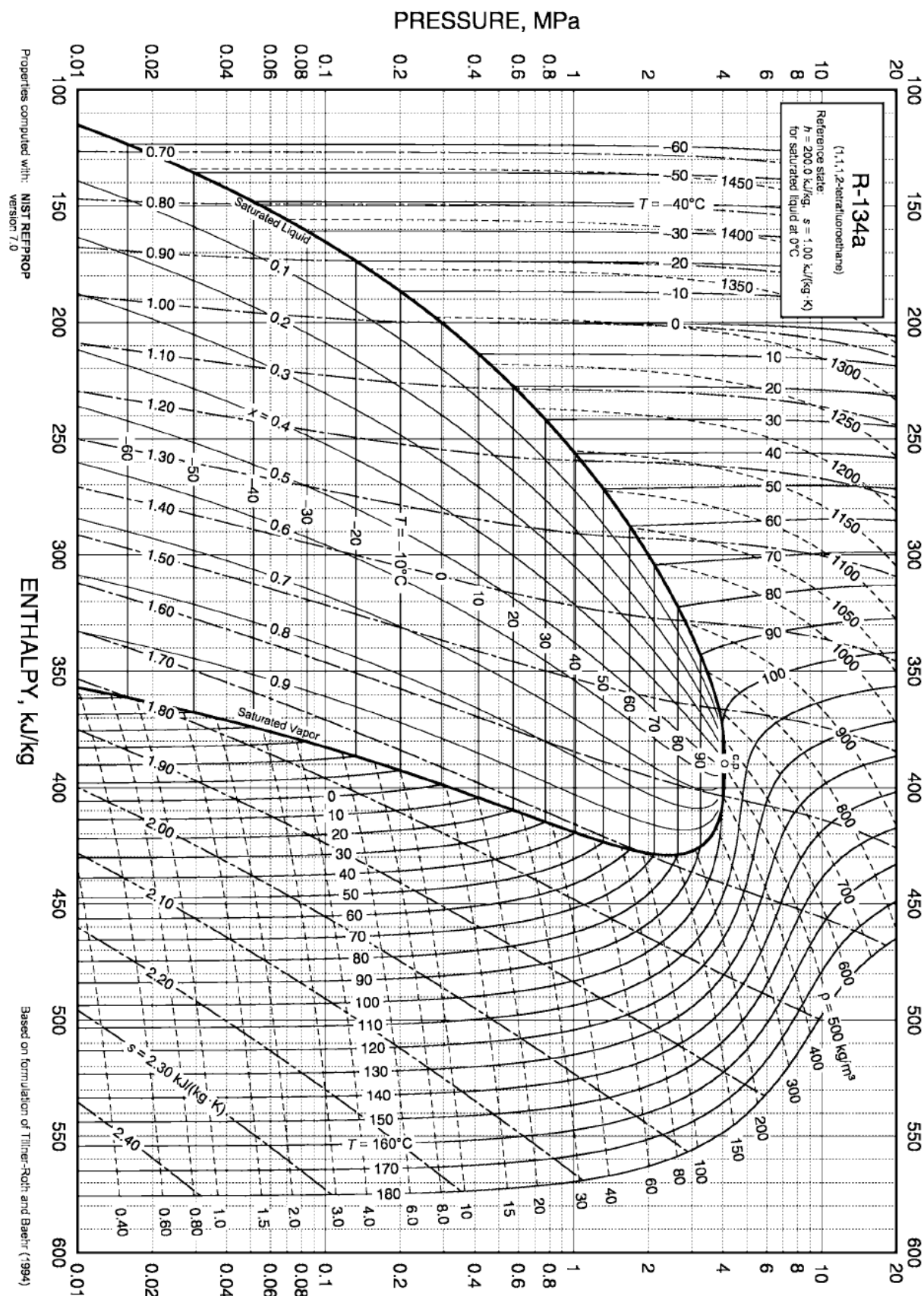
Ambient Temperature & Energy Demand Data

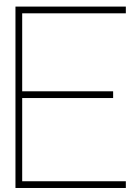
Hour\Day	7.02.2019			23.03.2019			7.05.2019			23.06.2019		
	Tamb (°C)	Industrial Hydrogen Demand (m³/s)	DHN Demand (m³/s)	Tamb (°C)	Industrial Hydrogen Demand (m³/s)	DHN Demand (m³/s)	Tamb (°C)	Industrial Hydrogen Demand (m³/s)	DHN Demand (m³/s)	Tamb (°C)	Industrial Hydrogen Demand (m³/s)	DHN Demand (m³/s)
00:00	6.8	0.00378603	4.82	8.6	0.003721860	4.64	5.3	0.0038395050	4.97	16.6	0.003436660	3.84
01:00	6.9	0.00378247	4.81	8.8	0.003714730	4.62	5.5	0.0038323750	4.95	17	0.003422400	3.8
02:00	7.3	0.00376821	4.77	8.8	0.003714730	4.62	5	0.0038502000	5	16.6	0.003436660	3.84
03:00	7.8	0.00375038	4.72	8.7	0.003718295	4.63	5.1	0.0038466350	4.99	16	0.003458050	3.9
04:00	8.1	0.00373969	4.69	8.7	0.003718295	4.63	4.9	0.0038537650	5.01	15.5	0.003475875	3.95
05:00	8.8	0.00371473	4.62	9	0.003707600	4.6	4.9	0.0038537650	5.01	15	0.003493700	4
06:00	9	0.00370760	4.6	9.2	0.003700470	4.58	5.3	0.0038395050	4.97	14.9	0.003497265	4.01
07:00	7.4	0.00376464	4.76	9.1	0.003704035	4.59	6.1	0.0038109850	4.89	16.3	0.003447355	3.87
08:00	6.8	0.00378603	4.82	9.3	0.003696905	4.57	8	0.0037432500	4.7	17.8	0.003393880	3.72
09:00	6.7	0.00378960	4.83	9.4	0.003693340	4.56	9.3	0.0036969050	4.57	19.9	0.003319015	3.51
10:00	7.1	0.00377534	4.79	9.3	0.003696905	4.57	11.5	0.0036184750	4.35	22.2	0.003237020	3.28
11:00	7.8	0.00375038	4.72	9.4	0.003693340	4.56	10.3	0.0036612550	4.47	24.4	0.003158590	3.06
12:00	8.1	0.00373969	4.69	9.1	0.003704035	4.59	12.5	0.0035828250	4.25	23.3	0.003197805	3.17
13:00	8.6	0.00372186	4.64	9.7	0.003682645	4.53	13.5	0.0035471750	4.15	22.8	0.003215630	3.22
14:00	8.6	0.00372186	4.64	9.9	0.003675515	4.51	12.7	0.0035756950	4.23	24.2	0.003165720	3.08
15:00	8.2	0.00373612	4.68	9.9	0.003675515	4.51	14	0.0035293500	4.1	24	0.003172850	3.1
16:00	7.8	0.00375038	4.72	9.4	0.003693340	4.56	14.6	0.0035079600	4.04	28.2	0.003137200	3
17:00	7.2	0.00377177	4.78	9.2	0.003700470	4.58	14.4	0.0035150900	4.06	28.7	0.003137200	3
18:00	7	0.00377890	4.8	8.2	0.003736120	4.68	14.6	0.0035079600	4.04	28.6	0.003137200	3
19:00	6.9	0.00378247	4.81	7.2	0.003771770	4.78	14.1	0.0035257850	4.09	27.8	0.003137200	3
20:00	6.7	0.00378960	4.83	6.9	0.003782465	4.81	13.5	0.0035471750	4.15	27.2	0.003137200	3
21:00	6.5	0.00379673	4.85	6.5	0.003796725	4.85	12.2	0.0035935200	4.28	26.4	0.003137200	3
22:00	6.4	0.00380029	4.86	5.8	0.003821680	4.92	11.2	0.0036291700	4.38	24.9	0.003140765	3.01
23:00	6.3	0.00380386	4.87	5.1	0.003846635	4.99	11.1	0.0036327350	4.39	24.2	0.003165720	3.08
Average	7.45	0.003762858	4.76	8.55	0.003723643	4.65	9.98	0.0036725	4.50	21.77	0.003277423	3.39

Hour\Day	7.08.2019			23.09.2019			7.11.2019			23.12.2019		
	Tamb (°C)	Industrial Hydrogen Demand (m³/s)	DHN Demand (m³/s)	Tamb (°C)	Industrial Hydrogen Demand (m³/s)	DHN Demand (m³/s)	Tamb (°C)	Industrial Hydrogen Demand (m³/s)	DHN Demand (m³/s)	Tamb (°C)	Industrial Hydrogen Demand (m³/s)	DHN Demand (m³/s)
00:00	18.6	0.003365360	3.64	16.1	0.003454485	3.89	7.1	0.003775335	4.79	8.6	0.00372186	4.64
01:00	18.7	0.003361795	3.63	16	0.00345805	3.9	6.8	0.00378603	4.82	8.7	0.003718295	4.63
02:00	18.4	0.003372490	3.66	15.9	0.003461615	3.91	6.1	0.003810985	4.89	8.9	0.003711165	4.61
03:00	18.5	0.003368925	3.65	15.9	0.003461615	3.91	6.2	0.00380742	4.88	8.7	0.003718295	4.63
04:00	18.3	0.003376055	3.67	15.8	0.00346518	3.92	6.1	0.003810985	4.89	8.4	0.00372899	4.66
05:00	18	0.003386750	3.7	15.7	0.003468745	3.93	7.2	0.00377177	4.78	8.2	0.00373612	4.68
06:00	18	0.003386750	3.7	15.8	0.00346518	3.92	7.6	0.00375751	4.74	8.4	0.00372899	4.66
07:00	17.2	0.003415270	3.78	15.7	0.003468745	3.93	8	0.00374325	4.7	7.5	0.003761075	4.75
08:00	18.1	0.003383185	3.69	15.7	0.003468745	3.93	7.7	0.003753945	4.73	7.4	0.00376464	4.76
09:00	18.7	0.003361795	3.63	15.7	0.003468745	3.93	8.3	0.003732555	4.67	8.3	0.003732555	4.67
10:00	19.2	0.003343970	3.58	16	0.00345805	3.9	8.7	0.003718295	4.63	8.1	0.003739685	4.69
11:00	20.1	0.003311885	3.49	16.1	0.003454485	3.89	8.7	0.003718295	4.63	8.3	0.003732555	4.67
12:00	20.4	0.003301190	3.46	17.7	0.003397445	3.73	8.7	0.003718295	4.63	8.5	0.003725425	4.65
13:00	17.7	0.003397445	3.73	16.8	0.00342953	3.82	8.3	0.003732555	4.67	8.8	0.00371473	4.62
14:00	20.1	0.003311885	3.49	17.9	0.003390315	3.71	8.4	0.00372899	4.66	8.8	0.00371473	4.62
15:00	21.7	0.003254845	3.33	19.1	0.003347535	3.59	8.1	0.003739685	4.69	8.9	0.003711165	4.61
16:00	21.8	0.003251280	3.32	19.1	0.003347535	3.59	8.3	0.003732555	4.67	8.4	0.00372899	4.66
17:00	21.9	0.003247715	3.31	18.4	0.00337249	3.66	8.8	0.00371473	4.62	8.4	0.00372899	4.66
18:00	21.5	0.003261975	3.35	18.6	0.00336536	3.64	9.2	0.00370047	4.58	8.2	0.00373612	4.68
19:00	20.8	0.003286930	3.42	17.5	0.003404575	3.75	7.9	0.003746815	4.71	8.1	0.003739685	4.69
20:00	19.8	0.003322580	3.52	15.6	0.00347231	3.94	7.4	0.00376464	4.76	8.5	0.003725425	4.65
21:00	19	0.003351100	3.6	15	0.0034937	4	7.2	0.00377177	4.78	9	0.0037076	4.6
22:00	19	0.003351100	3.6	13.8	0.00353648	4.12	6.9	0.003782465	4.81	8.6	0.00372186	4.64
23:00	18.9	0.003354665	3.61	15.8	0.00346518	3.92	6.5	0.003796725	4.85	8	0.00374325	4.7
Average	19.35	0.003338623	3.57	16.49	0.003440671	3.85	7.68	0.003754836	4.73	8.40	0.00372884	4.66

D

R134a Pressure - Enthalpy Table





Key Modelling Assumptions

E.1. Power-to-Gas

- Electrolyser
 - Electrolyser cells are assembled into stacks and connected in parallel for 50 MW capacity.
 - Concentration overpotential of electrolyser cell is ignored.
 - Ideal gas behaviour is assumed.
 - Temperature of the water in contact with the cell membrane is assumed to be uniform in the stack.
- Storage
 - Constant temperature and pressure inside the hydrogen storage tank.
 - Static and dynamic losses are ignored.

E.2. Power-to-Heat

- Heat Pump
 - Influence of part load efficiency is ignored.
 - Heat exchangers are supposed at hot start in equilibrium with the external sources and heat exchange is ideal.
 - Refrigerant massflow inside heatpump is assumed to be constant.
 - Isenthalpic flow across the expansion valve; and isentropic efficiency for the compressor.
- Storage
 - Constant temperature and pressure inside the hydrogen storage tank.
 - Static and dynamic losses are ignored.
 - Uniform temperature in the hot water reservoir (stratification is not considered)
 - No external heat loss from the reservoir wall
 - The total amount of hot water in the reservoir is conserved (No water consumption during heating process).

E.3. Multi-Energy System

- Power converters are ideal.
- Grid is able to provide flexible capacity when necessary.

F

Modelica Power-to-Gas Model Parameters

Parameter	Value	Remark
V_{std}	1.23 V	Cell voltage at standard conditions
T_{std}	298.15 °C	Standard Temperature
F	96485 C/mol	Faraday constant
R	8.314 JK ⁻¹ mol ⁻¹	Ideal gas constant
P_{cat}	30 bar	Pressure at cathode side
P_{an}	30 bar	Pressure at anode side
α_{an}	0.7353	Charge transfer coefficient at anode
$\sigma_{mem,std}$	10.31	Membrane conductivity at standard temperature
C_{th}	162116 J/K	Thermal capacitance of electrolyser
R_{th}	0.0668 K/W	Thermal resistance of electrolyser
V_{tn}	1.48 V	Minimum energy in electricity to heat to perform electrolysis(V)
n_{cells}	60	Number of cells per stack
V	100 m ³	Storage capacity
S_{base}	50 MW	Base power of system
$A_{membrane}$	290 cm ²	Membrane area
δ_{mem}	178e-6 m	Membrane thickness
K_{gain}	18000	Controller gain

G

Modelica Power-to-Heat Model Parameters

Parameter	Value	Remark
\dot{m}	5 kg/s	Water massflow rate
c_p	4.190 kJ/(Kkg)	Specific heat of water at 70 °C
ρ	977.74 kg/m³	Water density at 70 °C
V	2400 m³	Storage capacity
S_{base}	50 MW	Base power of system
K_{gain}	5	Controller gain

Bibliography

- [1] Zon op de slufter: exploitant gezocht voor grootste drijvende zonnepark van nederland, May 2019. URL <https://www.portofrotterdam.com/nl/nieuws-en-persberichten/zon-op-de-slufter>.
- [2] The Future of Hydrogen. *The Future of Hydrogen*, (June), 2019. doi: 10.1787/1e0514c4-en.
- [3] World Energy Outlook 2019. *International Energy Agency*, 2019. ISSN 1387-1811. doi: DOE/EIA-0383(2012)U.S. URL <https://www.eia.gov/outlooks/aoe/pdf/aoe2019.pdf>.
- [4] Lamiaa Abdallah and Tarek El-Shennawy. Reducing carbon dioxide emissions from electricity sector using smart electric grid applications. *Journal of Engineering (United Kingdom)*, 2013, 2013. ISSN 23144912. doi: 10.1155/2013/845051.
- [5] Alliander; ECN. Demand and supply of flexibility in the power system of the Netherlands, 2015-2050. *Summary report of the FLEXNET project*, (November 2017):70, 2017.
- [6] P K S Ayivor, J L Rueda Torres, and Mart A M M van der Meijden. Modelling of Large Size Electrolyser for Electrical Grid Stability Studies - A Hierarchical Control Approach. *17th International Wind Integration Workshop*, (October), 2018.
- [7] Bjarne Bach, Jesper Werling, Torben Ommen, Marie Münster, Juan M. Morales, and Brian Elmegaard. Integration of large-scale heat pumps in the district heating systems of Greater Copenhagen. *Energy*, 107:321–334, 2016. ISSN 03605442. doi: 10.1016/j.energy.2016.04.029. URL <http://dx.doi.org/10.1016/j.energy.2016.04.029>.
- [8] John Barton, Sikai Huang, David Infield, Matthew Leach, Damiette Ogunkunle, Jacopo Torriti, and Murray Thomson. The evolution of electricity demand and the role for demand side participation, in buildings and transport. *Energy Policy*, 52:85–102, 2013. ISSN 03014215. doi: 10.1016/j.enpol.2012.08.040. URL <http://dx.doi.org/10.1016/j.enpol.2012.08.040>.
- [9] Morten B. Blarke. Towards an intermittency-friendly energy system: Comparing electric boilers and heat pumps in distributed cogeneration. *Applied Energy*, 91(1):349–365, 2012. ISSN 03062619. doi: 10.1016/j.apenergy.2011.09.038. URL <http://dx.doi.org/10.1016/j.apenergy.2011.09.038>.
- [10] Andreas Bloess, Wolf Peter Schill, and Alexander Zerrahn. Power-to-heat for renewable energy integration: A review of technologies, modeling approaches, and flexibility potentials. *Applied Energy*, 212 (December 2017):1611–1626, 2018. ISSN 03062619. doi: 10.1016/j.apenergy.2017.12.073.
- [11] Carsten Bode and Gerhard Schmitz. Dynamic simulation and comparison of different configurations for a coupled energy system with 100% renewables. *Energy Procedia*, 155:412–430, 2018. ISSN 18766102. doi: 10.1016/j.egypro.2018.11.037. URL <https://doi.org/10.1016/j.egypro.2018.11.037>.
- [12] B. O. Bolaji and Z. Huan. Energy performance of eco-friendly RE170 and R510A refrigerants as alternatives to R134a in vapour compression refrigeration system. *Proceedings of the 9th Conference on the Industrial and Commercial Use of Energy, ICUE 2012*, (July):139–146, 2012.
- [13] Kenneth Bruninx, Dieter Patteeuw, Erik Delarue, Lieve Helsen, and William D’Haeseleer. Short-term demand response of flexible electric heating systems: The need for integrated simulations. *International Conference on the European Energy Market, EEM*, (March), 2013. ISSN 21654077. doi: 10.1109/EEM.2013.6607333.
- [14] Van Hai Bui, Akhtar Hussain, and Hak Man Kim. A multiagent-based hierarchical energy management strategy for multi-microgrids considering adjustable power and demand response. *IEEE Transactions on Smart Grid*, 9(2):1323–1333, 2018. ISSN 19493053. doi: 10.1109/TSG.2016.2585671.

- [15] Xinyu Chen, Xi Lu, Michael B. McElroy, Chris P. Nielsen, and Chongqing Kang. Synergies of wind power and electrified space heating: Case study for Beijing. *Environmental Science and Technology*, 48(3):2016–2024, 2014. ISSN 0013936X. doi: 10.1021/es405653x.
- [16] Tullie Circle. *2013 ASHRAE Handbook—Fundamentals*. 2013. ISBN 1936504472.
- [17] Jonathan M. Cullen and Julian M. Allwood. The efficient use of energy: Tracing the global flow of energy from fuel to service. *Energy Policy*, 38(1):75–81, 2010. ISSN 03014215. doi: 10.1016/j.enpol.2009.08.054. URL <http://dx.doi.org/10.1016/j.enpol.2009.08.054>.
- [18] Manuel Espinosa-López, Christophe Darras, Philippe Poggi, Raynal Glises, Philippe Baucour, André Rakotondrainibe, Serge Besse, and Pierre Serre-Combe. Modelling and experimental validation of a 46 kW PEM high pressure water electrolyzer. *Renewable Energy*, 119:160–173, 2018. ISSN 18790682. doi: 10.1016/j.renene.2017.11.081.
- [19] Björn Felten, Jan Paul Baginski, and Christoph Weber. KWK-Mindest- und Maximaleinspeisung - Die Erzeugung von Zeitreihen für die Energiesystemmodellierung. (10), 2017.
- [20] R. García-Valverde, N. Espinosa, and A. Urbina. Simple PEM water electrolyser model and experimental validation. *International Journal of Hydrogen Energy*, 37(2):1927–1938, 2012. ISSN 03603199. doi: 10.1016/j.ijhydene.2011.09.027.
- [21] Digvijay Gusain, Miloš Cvetković, and Peter Palensky. Energy flexibility analysis using FMUWorld. *2019 IEEE Milan PowerTech, PowerTech 2019*, 2019. doi: 10.1109/PTC.2019.8810433.
- [22] Kofi E. Hagan, Olufemi O. Oyebajo, Tarek Medalel Masaud, and Rajab Challoo. A probabilistic forecasting model for accurate estimation of PV solar and wind power generation. *2016 IEEE Power and Energy Conference at Illinois, PECI 2016*, pages 1–5, 2016. doi: 10.1109/PECI.2016.7459241.
- [23] Karsten Hedegaard, Brian Vad Mathiesen, Henrik Lund, and Per Heiselberg. Wind power integration using individual heat pumps - Analysis of different heat storage options. *Energy*, 47(1):284–293, 2012. ISSN 03605442. doi: 10.1016/j.energy.2012.09.030. URL <http://dx.doi.org/10.1016/j.energy.2012.09.030>.
- [24] Bongghi Hong and Robert W. Howarth. Greenhouse gas emissions from domestic hot water: Heat pumps compared to most commonly used systems. *Energy Science and Engineering*, 4(2):123–133, 2016. ISSN 20500505. doi: 10.1002/ese3.112.
- [25] Iea. Clean and efficient heat for industry – analysis. URL <https://www.iea.org/commentaries/clean-and-efficient-heat-for-industry>.
- [26] Intelligent Energy Europe. Guidelines for technical assessment of District Heating systems. URL www.ecoheat4cities.eu.
- [27] IRENA. *Hydrogen From Renewable Power: Technology outlook for the energy transition*. Number September. 2018. ISBN 9789292600778. URL www.irena.org.
- [28] Huiyong Kim, Mikyoung Park, and Kwang Soon Lee. One-dimensional dynamic modeling of a high-pressure water electrolysis system for hydrogen production. *International Journal of Hydrogen Energy*, 38(6):2596–2609, 2013. ISSN 03603199. doi: 10.1016/j.ijhydene.2012.12.006. URL <http://dx.doi.org/10.1016/j.ijhydene.2012.12.006>.
- [29] Jan Christian Koj, Christina Wulf, and Petra Zapp. Environmental impacts of power-to-X systems - A review of technological and methodological choices in Life Cycle Assessments. *Renewable and Sustainable Energy Reviews*, 112(November 2018):865–879, 2019. ISSN 18790690. doi: 10.1016/j.rser.2019.06.029. URL <https://doi.org/10.1016/j.rser.2019.06.029>.
- [30] Fabian Levihn. CHP and heat pumps to balance renewable power production: Lessons from the district heating network in Stockholm. *Energy*, 137:670–678, 2017. ISSN 03605442. doi: 10.1016/j.energy.2017.01.118. URL <https://doi.org/10.1016/j.energy.2017.01.118>.
- [31] Introduction Low-carbon. Netherlands Government Strategy on Hydrogen. *Report*, (387):1–14, 2020.

- [32] Peter D. Lund, Juuso Lindgren, Jani Mikkola, and Jyri Salpakari. Review of energy system flexibility measures to enable high levels of variable renewable electricity. *Renewable and Sustainable Energy Reviews*, 45:785–807, 2015. ISSN 13640321. doi: 10.1016/j.rser.2015.01.057. URL <http://dx.doi.org/10.1016/j.rser.2015.01.057>.
- [33] Pierluigi Mancarella. MES (multi-energy systems): An overview of concepts and evaluation models. *Energy*, 65:1–17, 2014. ISSN 03605442. doi: 10.1016/j.energy.2013.10.041. URL <http://dx.doi.org/10.1016/j.energy.2013.10.041>.
- [34] Pierluigi Mancarella and Gianfranco Chicco. Integrated energy and ancillary services provision in multi-energy systems. *Proceedings of IREP Symposium: Bulk Power System Dynamics and Control - IX Optimization, Security and Control of the Emerging Power Grid, IREP 2013*, (ii), 2013. doi: 10.1109/IREP.2013.6629423.
- [35] Luis Gabriel Marín, Mark Sumner, Diego Muñoz-Carpintero, Daniel Köbrich, Seksak Pholboon, Doris Sáez, and Alfredo Núñez. Hierarchical energy management system for microgrid operation based on robust model predictive control. *Energies*, 12(23), 2019. ISSN 19961073. doi: 10.3390/en12234453.
- [36] B. V. Mathiesen and H. Lund. Comparative analyses of seven technologies to facilitate the integration of fluctuating renewable energy sources. *IET Renewable Power Generation*, 3(2):190–204, 2009.
- [37] Modelica Association. Modelica Language Specification. 2017.
- [38] Mohammad Mohammadi, Younes Noorollahi, Behnam Mohammadi-ivatloo, and Hossein Yousefi. Energy hub: From a model to a concept – A review. *Renewable and Sustainable Energy Reviews*, 80 (December 2016):1512–1527, 2017. ISSN 18790690. doi: 10.1016/j.rser.2017.07.030.
- [39] Theresa Müller and Dominik Möst. Demand Response Potential: Available when Needed? *Energy Policy*, 115(February 2017):181–198, 2018. ISSN 03014215. doi: 10.1016/j.enpol.2017.12.025. URL <https://doi.org/10.1016/j.enpol.2017.12.025>.
- [40] Pierre Olivier, Cyril Bourasseau, and Pr Belkacem Bouamama. Low-temperature electrolysis system modelling: A review. *Renewable and Sustainable Energy Reviews*, 78(February):280–300, 2017. ISSN 18790690. doi: 10.1016/j.rser.2017.03.099.
- [41] Kazuo Onda, Toshio Murakami, Takeshi Hikosaka, Misaki Kobayashi, Ryouhei Notu, and Kohei Ito. Performance Analysis of Polymer-Electrolyte Water Electrolysis Cell at a Small-Unit Test Cell and Performance Prediction of Large Stacked Cell. *Journal of The Electrochemical Society*, 149(8):A1069, 2002. ISSN 00134651. doi: 10.1149/1.1492287.
- [42] Poul Alberg Østergaard. Comparing electricity, heat and biogas storages' impacts on renewable energy integration. *Energy*, 37(1):255–262, 2012. ISSN 03605442. doi: 10.1016/j.energy.2011.11.039. URL <http://dx.doi.org/10.1016/j.energy.2011.11.039>.
- [43] Peter Palensky and Dietmar Dietrich. Demand side management: Demand response, intelligent energy systems, and smart loads. *IEEE Transactions on Industrial Informatics*, 7(3):381–388, 2011. ISSN 15513203. doi: 10.1109/TII.2011.2158841.
- [44] G. Papaefthymiou, B. Hasche, and C. Nabe. Potential of heat pumps for demand side management and wind power integration in the German electricity market. *IEEE Transactions on Sustainable Energy*, 3(4): 636–642, 2012. ISSN 19493029. doi: 10.1109/TSTE.2012.2202132.
- [45] B. Parkinson, P. Balcombe, J. F Speirs, A. D. Hawkes, and K. Hellgardt. Levelized cost of CO₂ mitigation from hydrogen production routes. *Energy and Environmental Science*, 12(1):19–40, 2019. ISSN 17545706. doi: 10.1039/c8ee02079e. URL <http://dx.doi.org/10.1039/C8EE02079E>.
- [46] Raul Rodríguez Pearson. Pvsystems: A modelica library for photovoltaic system and power converter design. URL <https://raulrpearson.github.io/PVSystems/index.html#PVSystems>.
- [47] M. K. Petersen, K. Edlund, L. H. Hansen, J. Bendtsen, and J. Stoustrup. A taxonomy for modeling flexibility and a computationally efficient algorithm for dispatch in Smart Grids. *Proceedings of the American Control Conference*, pages 1150–1156, 2013. ISSN 07431619. doi: 10.1109/acc.2013.6579991.

- [48] Stefan Pfenninger and Iain Staffell. URL <http://www.renewables.ninja/>.
- [49] Stefan Pfenninger and Iain Staffell. Long-term patterns of European PV output using 30 years of validated hourly reanalysis and satellite data. *Energy*, 114:1251–1265, 2016. ISSN 03605442. doi: 10.1016/j.energy.2016.08.060. URL <http://dx.doi.org/10.1016/j.energy.2016.08.060>.
- [50] Heat Pumps, I N Combination, With District, Increases Energy, and Efficiency At. Heat pumps in combination with district heating increases energy efficiency at hammarbyverket.
- [51] Jonathan Reynolds, Muhammad Waseem Ahmad, and Yacine Rezgui. Holistic modelling techniques for the operational optimisation of multi-vector energy systems. *Energy and Buildings*, 169:397–416, 2018. ISSN 03787788. doi: 10.1016/j.enbuild.2018.03.065. URL <https://doi.org/10.1016/j.enbuild.2018.03.065>.
- [52] Rijkswaterstaat. Nieuw windpark maasvlakte 2, Mar 2020. URL <https://www.rijkswaterstaat.nl/nieuws/2020/03/ministerie-infrastructuur-en-waterstaat-verduurzaamt-met-nieuw-windpark-tweede-maasvlakte.aspx>.
- [53] Paul Schott, Johannes Sedlmeir, Nina Strobel, Thomas Weber, Gilbert Fridgen, and Eberhard Abele. A generic data model for describing flexibility in power markets. *Energies*, 12(10):1–29, 2019. ISSN 19961073. doi: 10.3390/en12101893.
- [54] Iain Staffell and Stefan Pfenninger. Using bias-corrected reanalysis to simulate current and future wind power output. *Energy*, 114:1224–1239, 2016. ISSN 03605442. doi: 10.1016/j.energy.2016.08.068. URL <http://dx.doi.org/10.1016/j.energy.2016.08.068>.
- [55] Leon Thurner, Alexander Scheidler, Florian Schafer, Jan Hendrik Menke, Julian Dollichon, Friederike Meier, Steffen Meinecke, and Martin Braun. Pandapower - An Open-Source Python Tool for Convenient Modeling, Analysis, and Optimization of Electric Power Systems. *IEEE Transactions on Power Systems*, 33(6):6510–6521, 2018. ISSN 08858950. doi: 10.1109/TPWRS.2018.2829021.
- [56] Bart W. Tuinema, Ebrahim Adabi, Patrick K.S. Ayivor, Víctor García Suárez, Lian Liu, Arcadio Perilla, Zameer Ahmad, José Luis Rueda Torres, Mart A.M.M. Van Der Meijden, and Peter Palensky. Modelling of large-sized electrolyzers for realtime simulation and study of the possibility of frequency support by electrolyzers. *IET Generation, Transmission and Distribution*, 14(10):1985–1992, 2020. ISSN 17518687. doi: 10.1049/iet-gtd.2019.1364.
- [57] Andreas Ulbig, Matthias A Bucher, and Göran Andersson. Operational Flexibility of Power Systems. In *Renewable Energy Integration*, pages 201–216. Elsevier, 2017. ISBN 9780128095928. doi: 10.1016/B978-0-12-809592-8.00015-9. URL <https://linkinghub.elsevier.com/retrieve/pii/B9780128095928000159>.
- [58] United Nations. Summary of the Paris Agreement. *United Nations Framework Convention on Climate Change*, pages 27–52, 2015. URL <http://bigpicture.unfccc.int/#content-the-paris-agreement>.
- [59] L. Vanfretti, T. Rabuzin, M. Baudette, and M. Murad. iTesla Power Systems Library (iPSL): A Modelica library for phasor time-domain simulations. *SoftwareX*, 5(September 2007):84–88, 2016. ISSN 23527110. doi: 10.1016/j.softx.2016.05.001. URL <http://dx.doi.org/10.1016/j.softx.2016.05.001>.
- [60] Clara Verhelst, Filip Logist, Jan Van Impe, and Lieve Helsen. Study of the optimal control problem formulation for modulating air-to-water heat pumps connected to a residential floor heating system. *Energy and Buildings*, 45:43–53, 2012. ISSN 03787788. doi: 10.1016/j.enbuild.2011.10.015. URL <http://dx.doi.org/10.1016/j.enbuild.2011.10.015>.
- [61] John Webster and Carsten Bode. Implementation of a Non-Discretized Multiphysics PEM Electrolyzer Model in Modelica. *Proceedings of the 13th International Modelica Conference, Regensburg, Germany, March 4–6, 2019*, 157:833–840, 2019. doi: 10.3384/ecp19157833.
- [62] Jens Weibezahn. Data Documentation 92: Electricity, Heat, and Gas Sector Data for Modeling the German System. *DIW Berlin*, 2017, (ISSN 1861-1532), 2017.

- [63] Edmund Widl, Tobias Jacobs, Daniel Schwabeneder, Sebastien Nicolas, Daniele Basciotti, Sawsan Henein, Tae Gil Noh, Olatz Terreros, Anett Schuelke, and Hans Auer. Studying the potential of multi-carrier energy distribution grids: A holistic approach. *Energy*, 153:519–529, 2018. ISSN 03605442. doi: 10.1016/j.energy.2018.04.047. URL <https://doi.org/10.1016/j.energy.2018.04.047>.
- [64] W. Yang, M.A. Wilkinson, and P.J. Tavner. Condition monitoring and fault diagnosis of a wind turbine synchronous generator drive train. *IET Renewable Power Generation*, 3(1):1–11, 2003. doi: 10.1049/iet-rpg.